Growth and Characterization of High-Performance Photorefractive $BaTiO_3$ Crystals

P.94

C. Warde, M. H. Garrett†, J. Y. Chang*, H. P. Jenssen† and H. L. Tuller*

Department of Electrical Engineering and Computer Science
*Department of Materials Science and Engineering
†Center for Materials Science and Engineering
Massachusetts Institute of Technology
Cambridge, MA, 02139 USA

Final Report

NASA GRANT No. NAG-1-996

December, 1991

Submitted to

National Aeronautics and Space Adminstration
Langley Research Center
Hampton, VA 23665

Attn. Sharon Welch

Abstract

Barium titanate has been used for many nonlinear optical applications primarily because it has high gain and high self-pumped phase conjugate reflectivities. However, barium titanate has had a relatively slow response time, and thus low sensitivity. Therefore, it has not been suited to real-time operation. In this report we will describe the modifications in crystal growth, doping, reduction and poling that have produced barium titanate crystals with the fastest photorefractive response time reported to date ~21 msec with a beam-coupling gain coefficient of 38.7 cm^{-1} and the highest sensitivity reported to date of 3.44 cm^3/kJ. The sensitivity of these barium titanate crystals is comparable to or greater than other photorefractive oxides. We will show, for the first time, beam-coupling in barium titanate at video frame rates. We infer from response time measurements that barium titanate has a phonon limited mobility. Also, photorefractive response time measurements as a function of the crystallographic orientation and grating wave vector for our cobalt-doped oxygen reduced crystals indicate that their faster response time arise because of an increase in the free carrier lifetime.

Contents

1 Introduction

The photorefractive effect (e.g., beam-coupling) and stimulated photorefractive scattering (e.g., self-pumped phase conjugation) are important nonlinear optical effects used for optical information processing. Barium titanate is a noncentrosymmetric ferroelectric single crystal at room temperature that is widely used to obtain either of these processes primarily because it has the largest known third-rank electrooptic tensor component for inorganic crystals to which the amplitude of both of these processes scale. The large electrooptic coefficient allows one to use barium titanate without applying high fields which is generally the case for other electrooptic materials such as gallium arsenide or bismuth silicon oxide. The application of high voltages to these materials results in a nonuniform space-charge field due to a blocking contact at one of the electrodes and thus non-optimal coupling. This is circumvented by using ac fields but this method usually requires bulky and expensive high voltage electronics. Barium titanate has found limited real time applications because the response time of the photorefractive effect in barium titanate was slow and thus the photorefractive sensitivity low. For example, in a beam-coupling measurement, the response time of barium titanate is usually around one second with an illumination intensity of 1 W/cm^2. The self-pumped phase conjugate rise time of barium titanate varies from three seconds to minutes depending on the illumination intensity and wavelength. The response time of these processes are clearly too slow to make practical the implementation of real-time optical information processing algorithms using barium titanate. Nevertheless, barium titanate is usually chosen by most researchers to demonstrate the potential of optical information processing because of its amplitude of response. Obviously, then, reducing the response time of the photorefractive effect and stimulated photorefractive scattering in barium titanate is an important goal.

The response time is approximately equal to the dielectric relaxation time [1] which is directly proportional to the dc dielectric constant and inversely proportional to the mobility-lifetime product.

We attempted (with success) to modify these material parameters to reduce the response time. In any practical device it is not only the response time of the nonlinear process but also the amplitude of the response. For example, for beam-coupling one may have a response time of milliseconds but only have a maximum gain coefficient (for diffusion processes) of tenths of an inverse centimeter. Thus, the speed of response is sufficient for real time operation but the detected signal change is relatively small (in some cases smaller than the absorption) and one will then encounter signal-to-noise problems. A figure of merit to compare different materials is the time to equivalent gain but this ignores absorption. A figure of merit that quantifies the gain, the rise time and the optical absorption of the material for a given input intensity is the photorefractive sensitivity or the index change per energy absorbed per unit volume [1]. This figure of merit was used extensively throughout the research reported herein to compare the changes in the photorefractive properties of barium titanate as a function of dopant and reduction state, to other photorefractive materials.

A fundamental limit of the response time is the time taken to deposit the energy within the material sufficient to form the index grating. This is called the photon limited response time [2]. This time is given by,

$$t_p = \left(\frac{h\nu}{e}\right)\left(\frac{\lambda}{\Lambda_g}\right)\left(\frac{\gamma}{\alpha}\right)\frac{2}{\pi\eta I Q}, \qquad (1)$$

where h is Planks constant, ν is the photon frequency, λ is the wavelength of light, γ is the gain coefficient, e is the electron's charge, Λ_g is the grating period, η is the quantum efficiency, I is the light intensity, and Q is the figure of merit equal to $n^3 r_{eff}/\varepsilon$ where n is the index of refraction, r_{eff} is the effective electrooptic coefficient, and ε is the dc dielectric constant. The figure of merit is a function of the variation in the effective electrooptic coefficient and the dc dielectric constant as

shown in Table 1. Shown in Table 2 are the photon limited response times computed with a quantum efficiency of 0.1, a grating period of 0.6 μm, a wavelength of light equal to 514.5 nm and an intensity of 1 W/cm^2. The first two $BaTiO_3$ response times are computed for 0°-cut crystals but with different polarizations. The third $BaTiO_3$ response time is computed for a 45°-cut crystal. One can see that the photon limited response time is around 1 msec for $BaTiO_3$ and similar to that of other photorefractive oxides such as potassium niobate $KNbO_3$ or bismuth silicon oxide BSO. We conclude, from this computation of the fundamental limit of the response time, that $BaTiO_3$ is far from this limit and therefore warrants research efforts to improve its response time which could potentially improve by three orders in magnitude as has been done for example with $KNbO_3$[3]. We also note that the beam-coupling gain is much higher in $BaTiO_3$ and if this material would have a response time sufficient to produce video frame rates it would be preferable to others photorefractive oxides for photorefractive applications since kilovolt fields are necessary to obtain high gain in materials like BSO or $KNbO_3$.

To minimize the response time we first investigated the change in the response time and sensitivity of barium titanate doped with strontium creating the mixed crystal barium strontium titanate [4]. We were motivated by previous work that had shown that the mobility was larger in the mixed crystal [5]. When growing this mixed crystal we found that the concentration of strontium could not be higher than 10% because concentration gradients due to the high segregation coefficient of strontium caused the boule to crack. It became evident in this phase of our research that the crystal growth technique used to obtain barium titanate, called top-seeded solution growth (TSSG), needed to be optimized with respect to the new furnace obtained for this project. We review our TSSG technique in section 3.

Our barium strontium titanate research has found that although the mobility may increase with larger concentrations of strontium but the dc dielectric constant also increases thus their ratio remains constant and we do not detect a systematic decrease in the response time with increased strontium concentrations in barium titanate. In addition, we find that the beam-coupling gain

remains approximately unchanged with strontium doping therefore there photorefractive sensitivity remains essentially unchanged. Thus, in this report we focus on the efforts that did improve the response time and sensitivity of cobalt-doped $BaTiO_3$.

Another approach to lower the response time of barium titanate is to oxygen-reduce the crystal. With this method other researchers have found that they can reduce the response time by an order of magnitude to 100 msec [6]. In fact, rather elegant theories have been developed that incorporate the change in the valence state of a multivalent interband impurity as a function of the oxygen partial pressure and predict that there is a reduction level that will produce a crystal that has a faster response time with high gain near the "compensation point" [7]. However, in most studies reported the beam-coupling gain is suppressed with reduction and thus the sensitivity of the material remains unchanged or even diminishes. The photorefractive theories used to help predict the compensation point allow for the excitation of both holes and electrons. We have found that in most cases a single carrier and two active traps more accurately describe the trap species involved in the photorefractive effect in barium titanate [8]. These facts make predictions of the single-specie multivalent ion photorefractive theory and the predicted relationship between the oxygen concentration in the sample and the response time and gain tenable. In fact, we have found that the participation of two photoactive traps, deep-and-shallow or both shallow, in the photorefractive effect is the rule and not the exception and we lack evidence for hole-electron competition at the wavelength for which we made our measurements, 514.5 nm. However, it is easy to conceive how oxygen-reduction will reduce the response time by simply reducing the number density of deep level recombination centers thus increasing the free carrier lifetime.

Previous work reported in the literature shows that the *dark conductivity* of barium titanate is a function of the impurity content and oxidation or reduction state of the sample [9]. Large variations in the dark conductivity (1 to 10^{15} Ω–cm^{-1}) have been obtained through oxygen-reduction. In the past, high conductivity samples have been produced by various researchers. It

becomes difficult to pole or align the domains of these samples because of blocking contact effects, (i.e. the applied voltage gets dropped across a small region of the sample near the electrode and not across the bulk of the material). We have developed an etching and pulse poling technique, described in section 4, that allows us to pole these high conductivity samples and the technique significantly reduces the processing time.

There has not been a systematic study of the *photoconductivity* (to which the response time is inversely proportional) as a function of the oxygen partial pressure for barium titanate. Schunemann et al. [10] did reduce barium titanate over a large range of partial pressures. They found that there was an absorption peak at 690 nm in some of their samples and when reduced there was an absorption peak at 450 nm. They tentatively proposed that these features arose from nickel impurities. They determined the beam-coupling properties with 633 nm laser illumination where the photorefractive sensitivity is low and they did not quantify the response time of the material. Unfortunately, they did not quench their samples and thus the actual reduction state of the crystals are somewhat uncertain. Subsequent doping studies with nickel did not confirm their proposition.

We used the measurement of the photorefractive response time, inversely proportional to the mobility-lifetime product or photoconductivity, as a measure of the photoconductivity at various reduction states of cobalt-doped barium titanate (20 ppm). The absorption peak at 450 nm was induced with oxygen-reduction in this crystal. In fact, other nominally undoped samples also had the absorption peak at 450 nm but at different reduction levels than the cobalt-doped crystals. We found that all these samples had enhanced photorefractive sensitivity at 514.5 nm. We suspect that this absorption feature is associated with a reduction-induced intrinsic defect (i.e., oxygen vacancies, singly and doubly ionized) and that transition metal impurities play an important role as donor and recombination centers through their valence state changes induced by oxygen vacancies, e.g., $[Me^{3+}] + e \rightarrow [Me^{2+}]$. As we will discuss in the text of this report, our response time measurements indicate that with a specific reduction level the concentration of the recombination

centers [Me^{3+}] associated with the transition metal ion impurities must diminish and thus the free carrier lifetime must increase with a concomitant reduction of the photorefractive response time.

During this research we designed a new technique to measure the electrooptic and absorptive gain by determining the net gain in amplification and depletion (where we have eliminated intensity-dependent absorption effects). In addition, we determined the effect of light-induced absorption/transparency on the photorefractive effect and thus accurately determined the photorefractive sensitivity of oxygen-reduced barium titanate. We have been able to produce reduced samples of barium titanate that have the fastest response times reported to date (~34 msec @ 1 W/cm^2) and no change in the electrooptic gain (3.62 cm^{-1} when accessing r_{13}), thus higher sensitivities.

Equally important we have also found that the anisotropy of both the dc dielectric constant and the mobility-lifetime product allow one to reorient the crystal from its normal 0°-cut orientation to a 45°-cut orientation, (where the interaction can easily access r_{42}), with little or no change in the response time (*implying that the mobility is phonon limited*) but with a factor of 13 increase in the beam-coupling gain (to 38.7 cm^{-1}). The combination of oxygen-reduction and reorientation into a 45°-cut yields a barium titanate crystal with a ~21 msec response time and a 38.7 cm^{-1} gain coefficient with a photorefractive sensitivity of 3.44 cm^3/kJ [11]. This is to the best of our knowledge the highest reported to date (by several orders in magnitude). The sensitivity of these crystals are now comparable to potassium niobate and bismuth silicon oxide. In addition, these oxygen-reduced 45°-cut samples have high self-pumped phase conjugate reflectivities (>45%) and fast self-pumped phase conjugate rise times (0-90%) of 50 msec with 150 mW input power at a wavelength of 514.5 nm. The net effect of this research is that we have significantly improved the response time and sensitivity of barium titanate such that it will continue to be the preference for researchers. In addition and possibly most significantly, herein we report on beam-coupling at video frame rates in barium titanate, making the use barium titanate for the photorefractive effect practical for real-time optical information processing.

References

1. G. C. Valley and M. B. Klein, Opt. Eng. **22**(6), 704 (1983).

2. P. Yeh, Appl. Opt. **26**, 602 (1987).

3. P. Günter and A. Krumins, Appl. Phys. **23**, 199 (1980).

4. M. H. Garrett, J. Y. Chang, H. P. Jenssen, H. L. Tuller and C. Warde, "Top-Seeded Solution Growth and Photorefractive Characterization of Barium Strontium Titanate, $Ba_{1-x}Sr_xTiO_3$," Proceedings of the American Conference of Crystal Growth - 8, Vail, Colorado, July 1990.

5. B. M. Choi, H. L. Tuller, and D. Goldschmidt, Phys. Rev. B, Vol. 34, No.10, pp. 6972-6979, (1986).

6. M. Klein, Photorefractive Materials and their Applications, Eds. P. Günter and J.-P. Huignard Springer-Verlag, 195 (1988)

7. B. A. Wechsler and M. B. Klein, JOSA B Vol. 5, 1711 (1988).

8. M. H. Garrett, J. Y. Chang, H. P. Jenssen and C. Warde, "High Beam-Coupling Gain in Cobalt-Doped Barium Titanate, $BaTiO_3$:Co," Submitted to JOSA B.

9. N.-H. Chang, R. K. Sharma, and D. M. Smyth, J. Am. Cer. Soc., 556 (1981).

10. P. G. Schunemann, T. M. Pollak, Y. Yang, Y.-Y. Teng, and C. Wong, JOSA B Vol. 5, 1702 (1988).

11. M. H. Garrett, J. Y. Chang, H. P. Jenssen and C. Warde, "High Photorefractive Sensitivity in a n-type $BaTiO_3$ Crystal," Opt. Lett., Jan. 15, 1992.

Table 1. Index of refraction, effective electrooptic coefficient, dc dielectric constant, and figure of merit for various photorefractive oxide crystals.

Materials	n	r_{eff}	ε	Q (pm/V)	Pol.
$BaTiO_3$	2.488	19.5	150	2.0	o
$BaTiO_3$	2.424	90.7	150	8.6	e
45°-$BaTiO_3$	2.45	1206	1875	9.5	e
BSO	2.54	5	56	1.5	cir.
SBN	2.3	1340	3400	4.8	e
$LiNbO_3$	2.2	31	32	10.3	e
$KNbO_3$	2.3	380	240	19.3	e

Table 2. Photon limited response time for various photorefractive oxide crystals. Note that the response time limit is around 1 msec for all these crystals but the gain is significantly different because of differences in effective electrooptic coefficients.

Materials	n	r_{eff}	ε	Q (pm/V)	Pol.	t_p msec	gain cm^{-1}
$BaTiO_3$	2.488	19.5	150	2.0	o	0.66	3.0
$BaTiO_3$	2.424	94.5	150	8.61	e	0.73	15.0
$45°$-$BaTiO_3$	2.45	1261	1875	9.9	e	1.4	32.5
BSO	2.54	5	56	1.5	cir.	0.17	0.2
SBN	2.3	1340	3400	4.8	e	6.6	33
$KNbO_3$	2.3	380	240	19.3	e	0.13	2.5

λ=514.5 nm

2 Properties of Barium Titanate

2.1 Material Properties

Many physical properties of barium titanate, $BaTiO_3$ arise because the crystal is ferroelectric. The ferroelectricity occurs during a first order structural phase transition at 130.5 C (see Figure 1). A displacement of titanium and oxygen atoms changes the space group from cubic to tetragonal (see Figure 2). The ionic displacement distorts the unit cell that has a formulation ABO_3 which belongs to a family of crystals called perovskites. The asymmetric shift in ionic positions is caused by an increase in the local electric field caused by the spontaneous polarization which increases faster than the elastic restoring force on an ion in the crystal. This is called a polarization catastrophe and occurs, from a thermodynamic point of view, because it is energetically favorable. The tetragonal unit cell has dimensions **c**=4.036 Å and **a**=**b**=3.992 Å.

The band diagram of $BaTiO_3$ shown in Figure 3. At the center of the Brillouin zone the self-consistent field-multiple scattering-Xα (SCF-MS-Xα) technique [1] has determined the intrinsic electronic structure from TiO^{8-}_6 clusters to have the top of the valence band composed of oxygen 2p states and the conduction band to consist of 3d titanium states for both the cubic (O_h symmetry) and the tetragonal (C_{4v} symmetry). Barium energy levels lie well below the valence band and do not play a direct role in the intrinsic electronic structure. Most transition metal impurities produce energy levels in the bandgap which is approximately 3.1 eV. The role of intrinsic and extrinsic defects will be discussed in section 2.2 on defect chemistry.

The phase transition from cubic to tetragonal decreases the symmetry from the centrosymmetric m3m point group to the noncentrosymmetric point group 4mm. The asymmetry is manifested in the anisotropy of the dielectric constant, indices of refraction, band edge, mobility-lifetime product, and the electrooptic coefficients. Barium titanate has the largest known electrooptic coefficient of

inorganic crystals, unclamped r_{42}=1640 pm/V, and helps gives rise to large optical nonlinearities. The electrooptic coefficients are defined in terms of the optical dielectric impermeability tensor η_{ij}. The principal values of the impermeability tensor are inverse of the optical dielectric constants, ε_k, where the optical dielectric constant is equal to the square of the index of refraction, $n_k^2=\varepsilon_k$. In the principal coordinate system the variation of the indices of refraction with position is given in terms of the index ellipsoid:

$$\frac{x^2}{n_x^2}+\frac{y^2}{n_y^2}+\frac{z^2}{n_z^2}=1 \quad . \tag{1}$$

With the application of a field **E** there is a redistribution of the bond electrons and possibly a slight change in the ionic positions that leads to a change in the optical impermeability tensor defined as,

$$\eta_{ij}(\mathbf{E})-\eta_{ij}(0)\equiv\Delta\eta_{ij}=r_{ijk}E_k+s_{ijkl}E_kE_l. \tag{2}$$

The first term is called the linear electrooptic effect (Pockels Effect) with third-rank electrooptic coefficients r_{ijk} and the second term is the quadratic electrooptic effect (Kerr Effect) with fourth-rank electrooptic coefficient s_{ijkl}. The field strengths are usually small enough such that their effect on the ionic positions can be neglected and thus one may neglect the quadratic effect. Since the impermeability tensor is a symmetric tensor the indices i and j can be permutated which results in a contracted notation for r_{ijk} [2]. Considering the symmetry operations for the tetragonal 4mm point group the electrooptic tensor components of barium titanate in the contracted notation are r_{13}, r_{33} and r_{42}.

The identity matrix I is equal to the tensor product of the optical impermeability tensor and the optical dielectric tensor i.e.,

$$\eta\,\varepsilon = I. \tag{3}$$

Differentiation equation (3) we obtain,

$$d\eta\,\varepsilon + d\varepsilon\,\eta = 0. \tag{4}$$

In the principal axis coordinate system recall $n_k^2=\varepsilon_k$ and for small changes we have,

$$dn_k = \frac{1}{2n_k} d\varepsilon_k = -\varepsilon_k \cdot d\eta_k \cdot \varepsilon_k = -\frac{n^3}{2} r_{ijk} E_k \,. \tag{5}$$

This equation expresses the fact that the index of refraction will be modulated linearly with the electric field (the linear electrooptic effect) with proportionally constant $1/2n^3r_{ijk}$.

When light illuminates the crystal photoinduced charge diffuses from the most intense regions of illumination and is trapped in the darker regions. The redistribution of charge causes a spatial variation in electric field. From the linear electrooptic effect there is a concomitant change in the index of refraction. This is called the photorefractive effect. For illumination by two plane waves with an external half angle θ there is an interference pattern or grating generated with a period equal to $\Lambda_g=\lambda/2\sin\theta$ as shown in Figure 4. From Poissons equation there is a spatial phase shift of $\pi/2$ of the index grating with respect to the incident intensity pattern. This allows for the coherent diffraction of one beam into another called two-wave mixing or beam-coupling. Various material parameters relevant to the photorefractive effect are listed in Table 1. The dependence of the

energy transfer on incident angle, trap densities and crystallographic orientation will be described in sections 5.1 and 8.1.

2.2 Defect Chemistry

The defect chemistry of barium titanate plays an important role in determining its electrical and optical properties. Although barium titanate is a line compound it is grown from a solution of excess titanium dioxide. This introduces the possibility of the incorporation of excess titanium and oxygen. Titanium on barium sites would produce barium vacancies to maintain charge neutrality. Titanium may also possibly be incorporated in a 3+ valence state at the high growth temperatures ~1400 C, (not the usual 4+), which will induce oxygen vacancies. In addition, if transition metal ions, (which are usually acceptor ions with respect to the valence state of titanium), are present in the melt they are usually incorporated on titanium sites and help make the material p-type in the as-grown state. It is also possible to alter the stoichiometry of the as-grown crystal by oxidation or reduction. The electrical and optical properties are modulated with oxidation/reduction and these directly effect the photorefractive properties of barium titanate, i.e. the dark conductivity, the photoconductivity and the absorption. Next we will discuss defect modelling and see how acceptor-doping and oxygen-reduction control the dark conductivity and oxygen vacancy concentration in barium titanate. In section 6 we will describe the effect of oxygen-reduction on the absorption spectra of barium titanate. In section 7 we will describe how the photorefractive properties are optimized for specific reduction conditions.

The defect model described below is essentially that of Hagemann [3] and that discussed by Schunemann [4]. In the following discussion, equilibria is presented using Kroger-Vink notation [5]. Each species is identified by a symbol indicating the nature of the defect (e.g. V for vacancy A for acceptor); a subscript indicating the crystallographic site on which the defect is located; and a superscript denoting the charge of the site relative to that of the species normally occupying the site (^{x} = neutral, $'$ = -1, $^{\bullet}$ = +1).

Let us first consider the case of the undoped stoichiometric barium titanate with a Ba/Ti ratio of unity. A very simplified model can be based on the following assumptions: (1) intrinsic ionic disorder contributes negligibly to the defect structure; (2) all defects are fully ionized. At low oxygen partial pressures and elevated temperatures, oxygen vacancies would be created and balanced by the generation of mobile electrons according to the chemical reaction and law of mass action as,

$$O_O = V_O^{\cdot\cdot} + \frac{1}{2}O_2(g) + 2e^{\cdot}, \quad [V_O^{\cdot\cdot}]n^2 = K_1 P_{O_2}^{-1/2} \tag{1}$$

where K_1 is the equilibrium constant and is temperature dependent, and P_{O2} is oxygen partial pressure. Conservation of charge, mass and concentration has been observed. The first equation expresses the equality between oxygen on an oxygen site and the production of a doubly ionized oxygen liberating oxygen gas and leaving two electrons on the oxygen site for charge concentration. The second equation describes the relationship between the oxygen vacancy concentration, the free carrier density and the partial pressure of oxygen which are related by the rate constant K_1. The electroneutrality condition in this region would be approximated by,

$$n \approx 2[V_O^{\cdot\cdot}], \tag{2}$$

such that the material would exhibit n-type electrical conductivity given by,

$$\sigma_e = ne\mu_e = K_1' P_{O_2}^{-1/6} e\mu_e. \tag{3}$$

This equation predicts that the conductivity of pure stoichiometric barium titanate is a function of the partial pressure of oxygen and would vary as the -1/6 power.

At even higher oxygen partial pressure, once all the oxygen vacancies were effectively filled, pure stoichiometric barium titanate would behave simply as an intrinsic semiconductor with the electron-hole pairs given by

$$nil = h^{\cdot} + e' \text{ and, } np = K_2 = K_2' \exp(-E_g / kT), \tag{4}$$

where E_g is the energy gap, k is Boltzmann's constant and K'_2 is the product of the densities of state of the conduction and valence band. This model therefore predicts two regions of behavior; a conductivity that is oxygen partial pressure dependent and an intrinsic conductivity region.

Actual studies [6,7,8] of the defect chemistry of undoped barium titanate by means of equilibrium electrical conductivity measurement indicate an additional region of p-type conductivity for which this simple model does not account. Typical results are shown in Figure 5 [8], plotted as $\log(\sigma)$ versus $\log(P_{O2})$. The p-type conductivity is represented at high oxygen partial pressures as an increase in conductivity with increase P_{O2}. While at low P_{O2} the conductivity changes to n-type. The -1/4 and +1/4 dependence of $\log\sigma$ versus $\log P_{O2}$ observed for the n-type and p-type regions respectively are inconsistent with the above model which predicts a $\pm 1/6$ dependence.

These inconsistences can be explained by assuming the presence of a species with a net negative charge, i.e. acceptors. In the region of partial oxygen pressure where the total concentration of oxygen vacancies is fixed by acceptor impurities, the electroneutrality relation is given by

$$[A'_{Ti}] \approx 2[V_O^{\cdot\cdot}] \tag{5}$$

Substitution of equation into equation (1) gives

$$n = K_3 P_{O_2}^{-1/4} \tag{6}$$

which indicates a -1/4 power dependence with oxygen partial pressure.

At lower P_{O2} and high temperatures, the concentration of oxygen vacancies will exceed the extrinsic levels induced by acceptors and oxygen vacancies be compensated by electrons, as indicated by the simple model in which the power coefficient is -1/6. At higher P_{O2}, however, the extrinsically generated oxygen vacancies will begin to be partially filled according to the reaction,

$$V_O^{\cdot\cdot} + \frac{1}{2}O_2(g) = O_O^x + 2h^{\cdot}, \quad p^2 / [V_O^{\cdot\cdot}] = K_4 P_{O_2}^{1/2} \tag{7}$$

Substitution of equation yields,

$$p = K_5 P_{O_2}^{1/4}, \tag{8}$$

with a corresponding p-type conductivity,

$$\sigma_h = pe\mu_h = P_{O_2}^{1/4} e\mu_h \tag{9}$$

where is power coefficient is 1/4. At still higher oxygen partial pressures the acceptor generated oxygen vacancies could be sufficiently depressed to saturate the hole concentration at ,

$$p = [A']. \tag{10}$$

The defect chemistry of barium titanate grows still more complex when the acceptor impurities or dopants can exist in more than one stable valence state. Such is the case for transition metal

ions, in particular Cr, Mn, Fe, Co and Ni substituted at titanium sites. To account for acceptors in variable valence states the defect model must be expanded to include the acceptor ionization reactions,

$$A''_{Ti} = A'_{Ti} + e', \quad \frac{[A'_{Ti}]n}{[A''_{Ti}]} = K_6, \tag{11}$$

for more reducing conditions and,

$$A'_{Ti} = A^{x}_{Ti} + e', \quad \frac{[A^{x}_{Ti}]n}{[A'_{Ti}]} = K_7 \tag{12}$$

for more oxidizing conditions. The total electroneutrality condition is,

$$n + [A'_{Ti}] + 2[A''_{Ti}] = p + [V'_O] + 2[V''_O]. \tag{13}$$

The consequence of acceptors existing in variable valence states is that there are then two regimes in which the oxygen concentration is extrinsically controlled. Hagemann [9] measured the oxygen vacancy concentration as a function of oxygen partial pressure in undoped and acceptor-doped barium titanate annealing in the 1000 C as shown in Figure 6. Two distinct regions can be recognized: at medium and high oxygen partial pressures the oxygen vacancy concentration is controlled by the acceptor dopant, in accordance with the previous described oxygen compensation mechanism. For example, in cobalt-doped barium titanate, after reduction, for each two Co^{+3} ions changing to Co^{+2}, one oxygen vacancy is formed until nearly all of the valence state is +2. In addition, there is a constant oxygen vacancy concentration segment since nearly all acceptors are in the same valence state. This means that the formation of additional vacancies, by lowering the partial pressure, is hampered since energetically favorable acceptor states are no longer available

for trapping the electrons which are always generated together with the vacancies. In this regime, the charge balance condition requires

$$[A'_{Ti}] \approx 2[V_O^{\cdot\cdot}] \tag{14}$$

for the transition region from the tetravalent to the trivalent state or

$$[A'_{Ti}] + 2[A''_{Ti}] \approx 2[V_O^{\cdot\cdot}] \tag{15}$$

if trivalent and divalent acceptors are present. However, if the oxygen partial pressure is lowered beyond the limits set by acceptor amount, the intrinsic defects, i.e. oxygen vacancies and mobile electrons, become increasing important. In this intrinsic regime (similar to highly reduced pure stoichiometric barium titanate), the vacancy concentration is much larger than the acceptor concentration and the condition of charge balance is

$$n \approx 2[V_O^{\cdot\cdot}] \tag{16}$$

which is n type conductivity. In Figure 6 the intrinsic region is to the left of the knee of the change in slope and for the sample characterized by Hagemann it is at a partial pressure less than 10^{-10} atmospheres at 1000 C.

Our as-grown nominally undoped crystals were analyzed by Spark-Source Mass Spectroscopy and the total transition metal ion impurities were around 7 ppm where the [Fe] is approximately 2.5 ppm. In addition, electron paramagnetic resonance measurements were performed (particulary sensitive to sub ppm levels) at room temperature and liquid nitrogen temperature and confirmed these concentrations.

We heavily reduced the undoped sample and 20 ppm cobalt-doped samples as will be

discussed in section 6. In section 6 we also give the resulting changes in absorption with reduction. Our barium titanate samples have an absorption peak around 450 nm. Crystals with this feature have the fastest response time and highest photorefractive sensitivity reported to date.

References

1. F. M. Michel-Calendini, H. Chermette, J. Weber: J. Phys. **C13**, 1427 (1980).
2. A. Yariv, P. Yeh, *Optical Waves in Crystals*, J. Wiley and Sons, 222 1984.
3. H. -J. Hagemann, "Akzeptorionen in $BaTiO_3$ und $SrTiO_3$ und ihre Auswirkung auf die Eigenschaften von Titanatkeramiken", Ph. D Thesis, Rheinisch-Westfalischen Technischen Hochschule, Aachen (1980).
4. P. G. Schunemann, Master Thesis, Massachusetts Institute of Technology, Cambridge, MA (1987).
5. F. A. Kroger and H. J. Vink, " Relations between the concentrations of imperfections in crystalline solids", in Solid State Physics **3**, F. Seitz and D. Turnbull, eds., Academic Press, 307 (1956).
6. S. A. Long and R. N. Blumenthal, J. Amer. Cer. Soc. **54**, 515 (1971).
7. N. G. Eror and D. M. Smyth, J. Solid State Chemistry. **24**, 235 (1978).
8. N. -H. Chan, R. K. Sharma and D. M. Smyth, J. Amer. Cer. Soc. **64**, 556 (1981).
9. H. -J. Hagemann and D. Hennings, J. Amer. Cer. Soc. **64**, 590 (1981).

1460 C
Hexagonal -> Cubic

130.5 C
Cubic -> Tetragonal

5 C
Tetragonal -> Orthorhombic

-90 C
Orthorhombic -> Rhombohedral

Figure 1. Structural phase transitions of barium titanate, $BaTiO_3$.

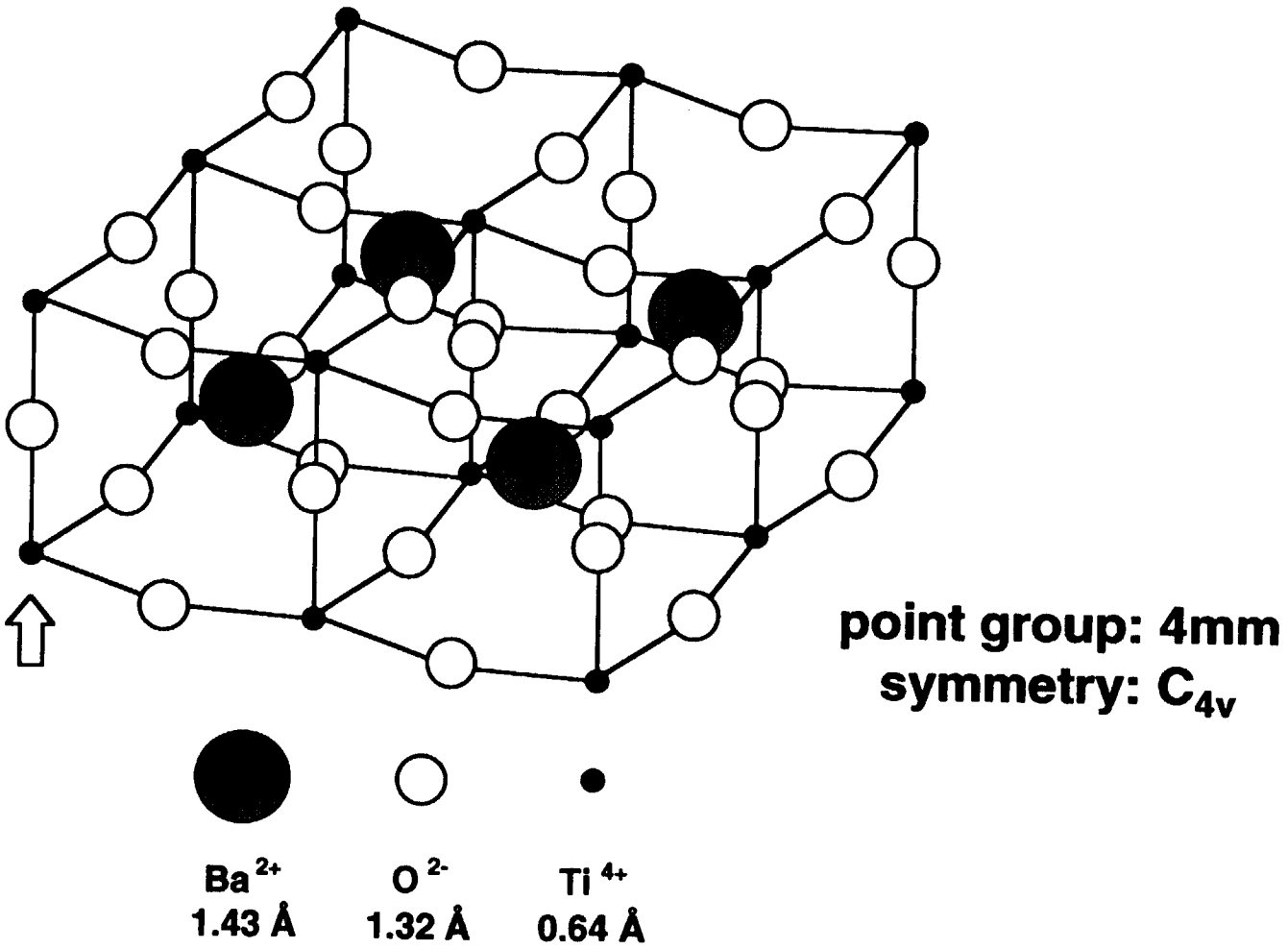

Figure 3. Diagram of several unit cells of barium titanate in the tetragonal phase with point group 4mm. The titanium atoms and oxygen atoms are displaced along the direction of the spontaneous polarization, the c-axis.

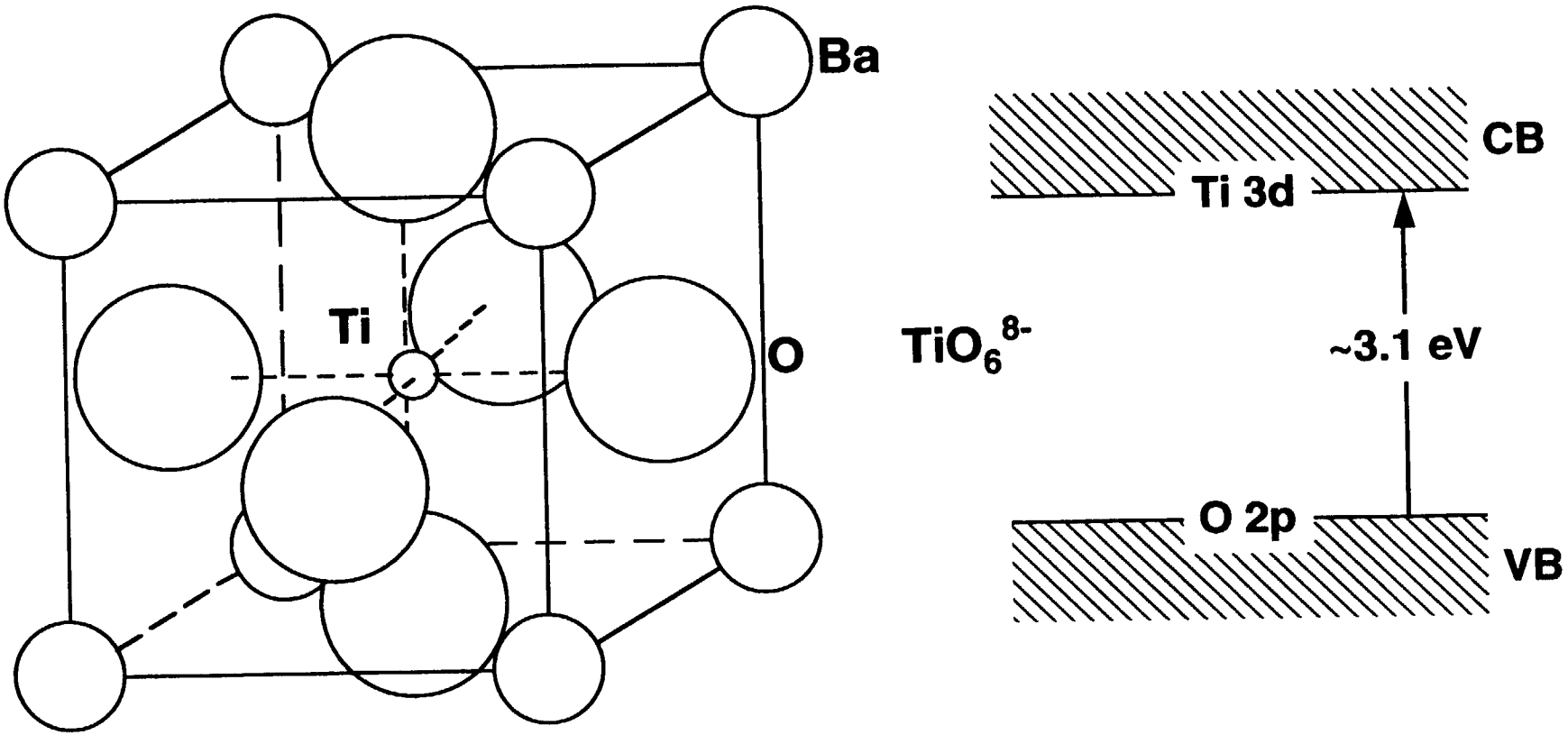

Figure 2. The unit cell of barium titanate. The oxygen octahedra surrounding the titanium are responsible for the intrinsic electrical conduction. The 2p orbitals of oxygen compose the valence band and the 3d orbitals of titanium are responsible for the conduction band.

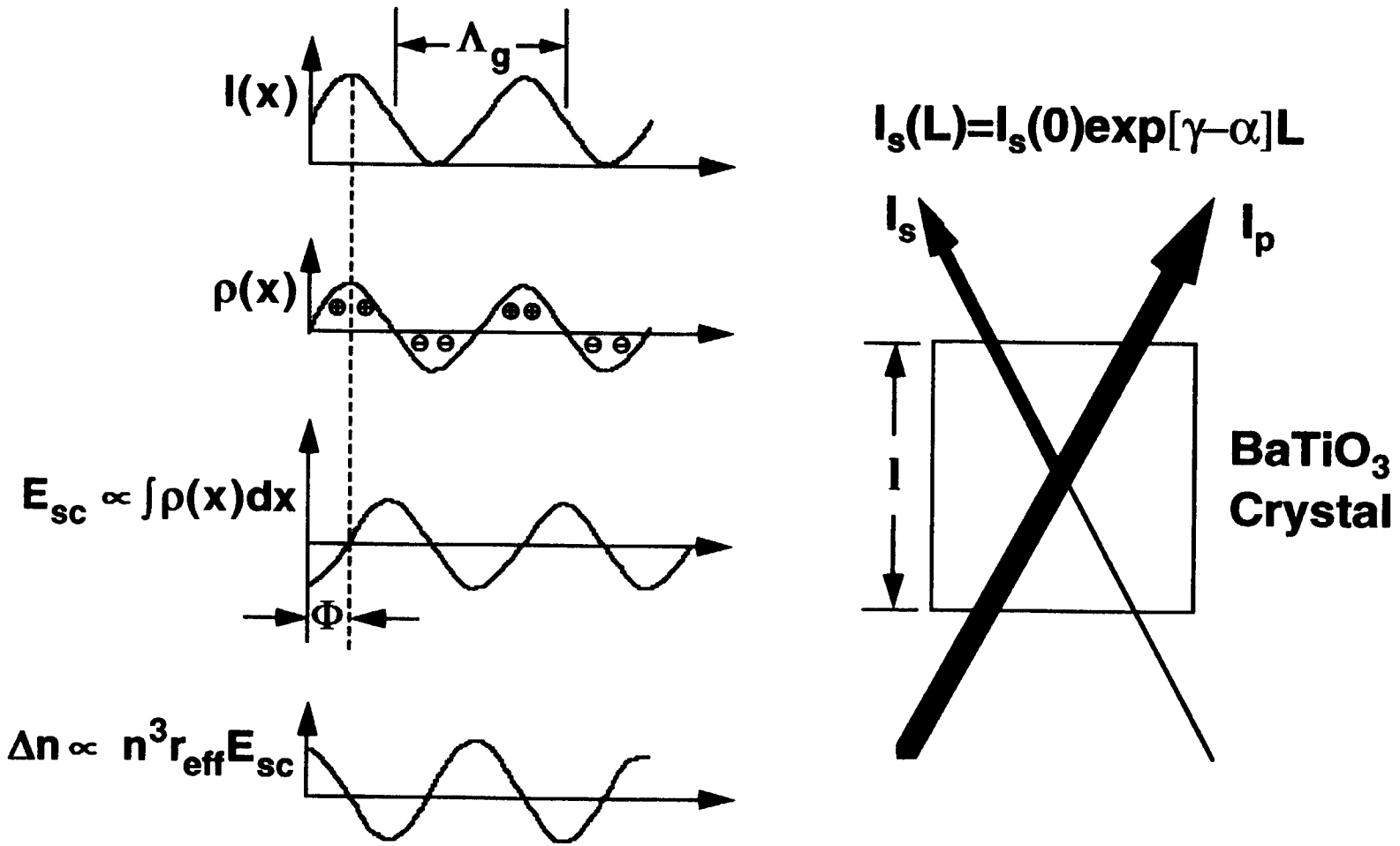

Figure 5. Pictoral description of the photorefractive effect. The spatial phase shift of $\pi/2$ of the index grating with respect to the intensity interference pattern induces an energy transfer from the pump beam I_p to the signal beam I_s called beam-coupling.

- **Band Gap ~3.1 eV**
- **Absorption 0.1-8 cm^{-1} (visible spectrum)**
- **Electrooptic Coefficients: r_{13}=19.5, r_{33}=97, r_{42}=1640 pm/V**
- **Indices of Refraction (514.5 nm): n_o=2.488, n_e=2.424**
- **Dielectric Constants: ε_a=3600, ε_c=150**
- **Conductivity: 10 - 10^{-16} $(\Omega\text{-cm})^{-1}$**
- **Photo-Induced Majority Carriers: holes (As-Grown)**
- **First-Order Phase Transition @ ~130 C**

Figure 4. List of the material properties of the ferroelectric $BaTiO_3$. Optical constants are given for 514.5 nm illumination.

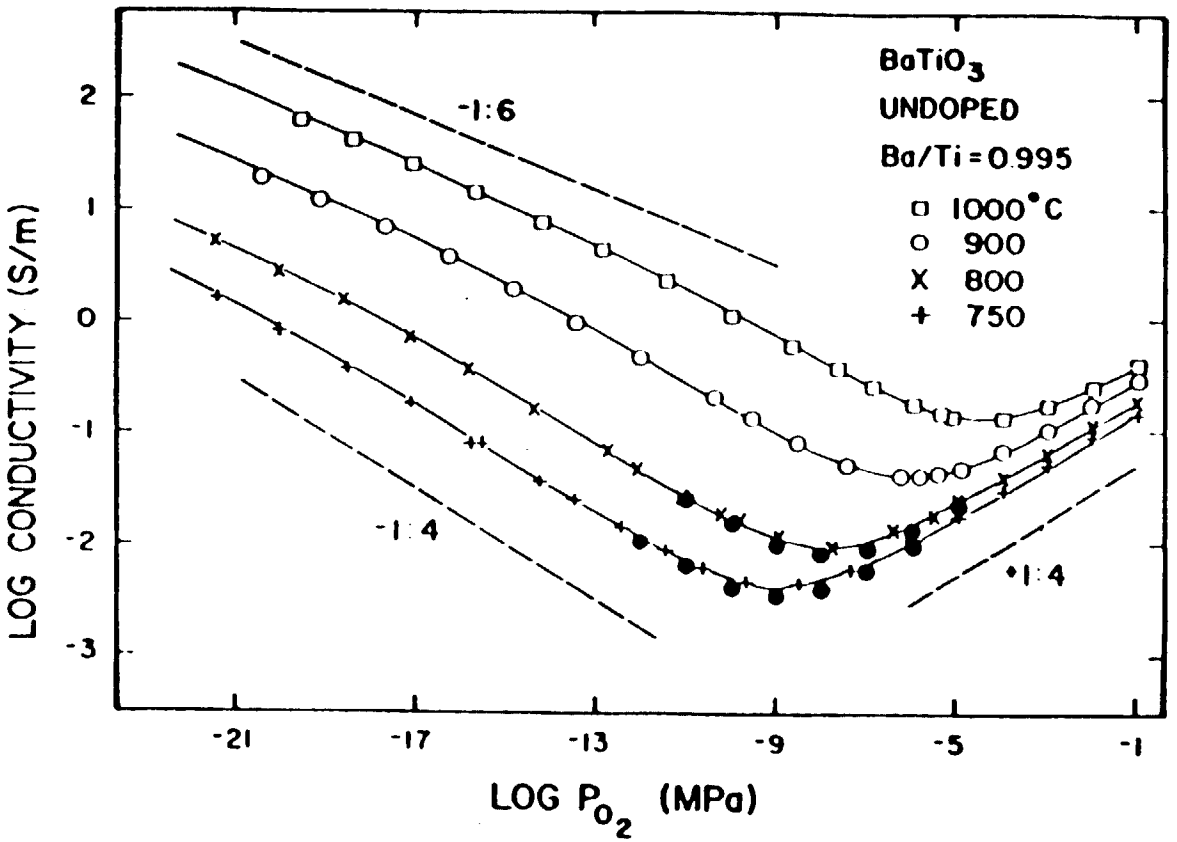

Figure 5. Typical equilibria conduction isotherms for undoped barium titanate [3].

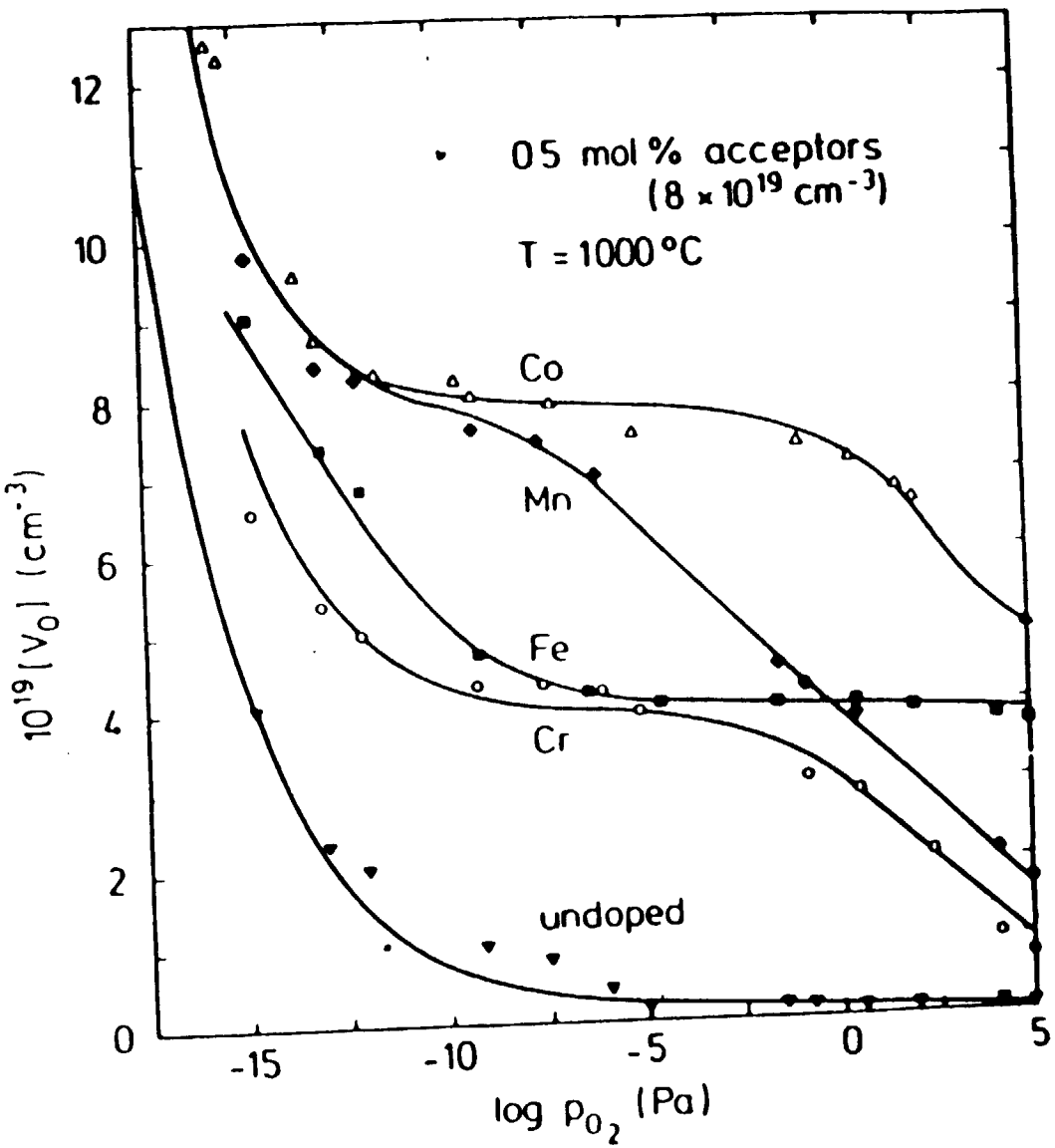

Figure 6. Oxygen vacancy concentration dependence with oxygen partial pressures of undoped and acceptor doped barium titanate [3].

3 Top-Seeded Solution Growth

The TSSG method evolved by first understanding the phase diagram of the BaO-TiO_2 system [1] as shown in Figure 1. The congruent melting point of barium titanate is approximately 1620 C at 50 mole % BaO and 50 mole % TiO_2. However, after growth from this melt and upon cooling a crystal from this temperature it under goes several phase transitions one of which is destructive, (hexagonal-to-cubic). To avoid these phase changes and produce large high quality samples a top-seed solution growth technique was developed at MIT in 1965 by V. Belruss [2]. The technique is essentially the precipitation of crystalline BT, ($BaTiO_3$), from a solution of excess titanium oxide. The crystallization results from a seeded and temperature induced quasi-equilibrium concentration adjustments.

The growth process is as follows: A charge with composition 66.6 mole % TiO_2 and 33.4 mole % BaO. According to the phase diagram, at 1395 C this composition will be in equilibrium with a solid of composition $BaTiO_3$, (vertical line). If the temperature of the melt is lowered the melt will precipitate, or nucleate onto a seed, an amount of solid of composition $BaTiO_3$ to adjust the melt composition to be in equilibrium at the new temperature. This growth process produces about 0.5 grams of BT for each degree of temperature decrease with a 400 gram melt. The growth must be terminated before the eutectic point at approximately 1320 C. The *key* concept to the successful growth of large mass high quality BT is the rate of precipitation of the solid. Solution growth is a diffusion limited process and thus has much slower growth rates than the Czochralski method. Any process or technique the produces a rapid deposition of material will reduce the quality of the resulting sample. This is especially true of barium titanate.

In practice several crystal growth parameters are adjusted to achieve high quality crystals. The steps taken to grow BT are shown in Figure 2. Initially several fillings of TiO_2 and $BaCO_3$ are needed to obtain an adequate volume of melt. For a 400 gram melt approximately 40 grams of BT

can be extracted. With the proper growth conditions we have been able to pull the maximum possible crystal mass. The melt is first "soaked" at a temperature well above the growth temperature to insure adequate mixing, (~1450 C for 24 hours). To induce crystalline growth and a single nucleated crystal the seed is "melted back" and several tenths of a millimeter of the seed is removed. The temperature is then lowered to a point where there is no melt back or growth on the seed. This is the "seeding" temperature. This is an essential step to obtain high quality samples. Recall that 1/2 gram of material is precipitated for each degree below the "seeding" temperature. If one starts the growth at a temperature below the seeding temperature the material will be suddenly precipitated onto the seed or some other part of the crucible. This type of growth will exceed the optimum rate of deposition and will encourage the formation of a "cap" and or multiple grain growth. In addition, growth of an unwanted crystal may be initiated and limit the useful yield.

We have developed a seeding technique that allows one to identify the "seeding" temperature within 1/2 C. Figure 3 is a plot of the amount of material melted away from the seed in a 15 minute interval as a function of the melt temperature. By using the digital stepper motors inherent high resolution we are able to determine the seed loss to within 0.05 mm. This is an extremely reliable and necessary technique to eliminate capping. It is essential that one approaches the seeding temperature from the high side, i.e. at temperatures greater than the seeding temperature. If one is too cool, (one has not melted back the seed), then it is necessary to raise the temperature well above the seeding temperature to ensure complete melting of all material. Air cooling has been commonly used by most BT crystal growers to induce nucleation. We have found that with the proper furnace design and growth processes it is unnecessary to use air cooling. In fact air cooling can be an unwanted variable since it can effectively change the "equilibrium" seeding temperature and produce a gradient of unknown magnitude that will be altered as the seed rod is translated. Both effects will lead to capping.

Capping can also be induced by the rate of expansion of the boule. Even if the proper seeding technique has been followed if one allows the boule to expand from the seed in planar fashion this

will induce capping. We have developed a sequence of computer controlled steps to control this rate as given in Figure 2. This has been taylored to our furnace which has been designed to reduce vertical and radial thermal gradients. In addition, a symmetric rotation of the seed and thus boule is also essential to minimizing capping and solution inclusions. We routinely used a rotation rate of 60 rpm. However, we also tried rotation rates as low as 20 rpm which altered the interface shape but not the crystal quality. As a final note we found it was *not* necessary to cool the sample at an exceedingly slow rate through the Curie temperature. After growth we used a cooling rate of -40 C/hr to room temperature. Shown in the Figure 4 ia a boule grown by the process we have outlined.

References

1. K. W. Kirby and B. A. Wechsler, J. Am. Ceram. Soc., 1991

2. V. Belruss, J. Kalnajs and A. Linz, Mat. Res. Bull. **6**, 899 (1971).

Paste in $BaTiO_3$ Phase Diagram

Figure 1. Phase diagram of barium titanate. This is a plot of the equilibrium relationship between temperature, liquid and solid compositions, Kirby and Wechsler [1].

Temperature Control Sequence

Event	Units	Duration	Delay
1	-.25 °C/hr	15 hrs	0
2	-.35 °C/hr	15 hrs	15 hrs
3	-.50 °C/hr	15 hrs	30 hrs
4	-.65 °C/hr	15 hrs	45 hrs
5	-.75 °C/hr	53 hrs	60 hrs

Translation Sequence

Event	Units	Duration	Delay
1	.1 mm/hr	10 hrs	0
2	.15 mm/hr	10 hrs	10 hrs
3	.2 mm/hr	10 hrs	20 hrs
4	.25 mm/hr	83 hrs	30 hrs

Figure 2. Top-seeded solution growth process used to grow barium titanate.

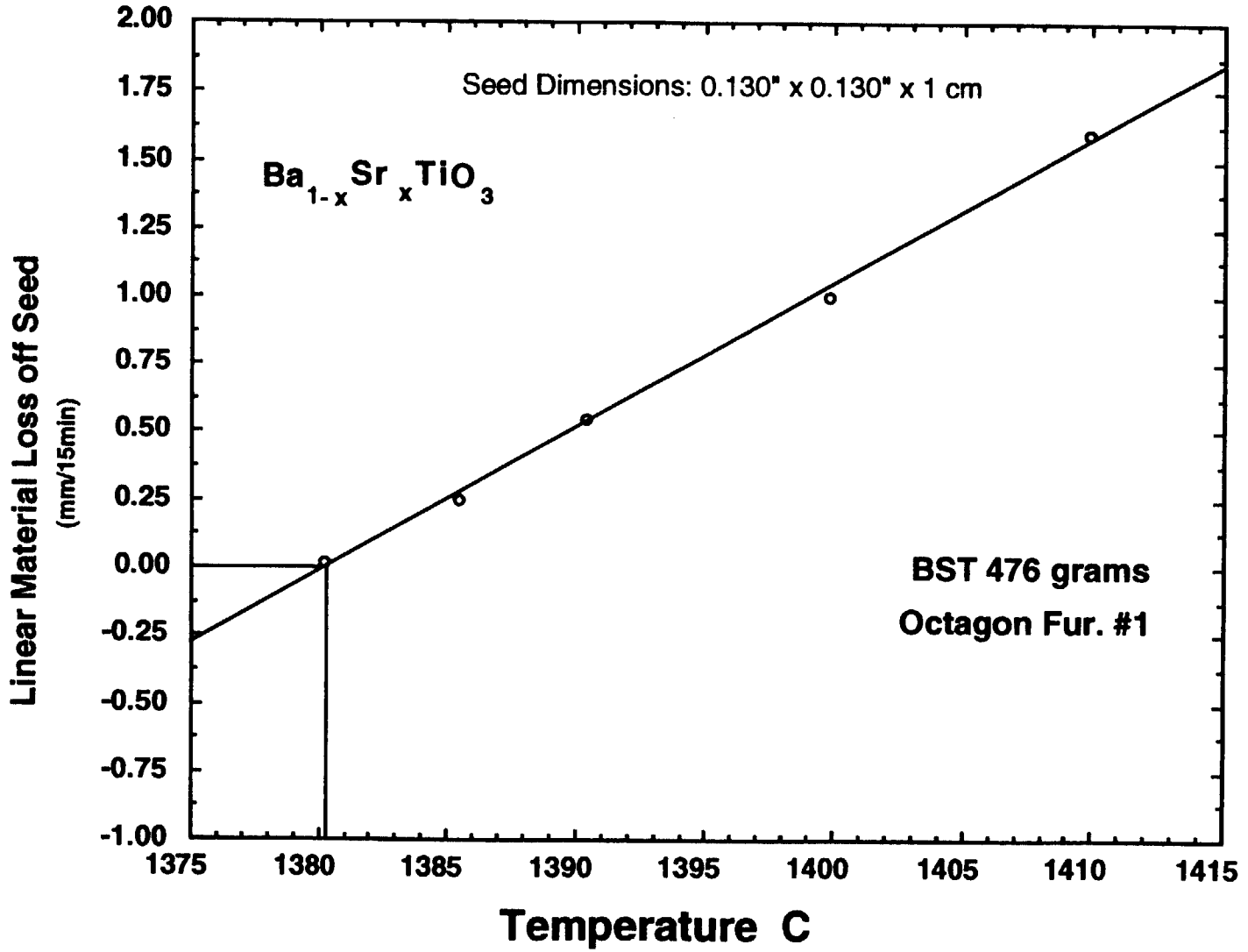

Figure 3. Plot of the amount of material loss from the seed as a function of temperature. This is used to accurately infer the seeding temperature for barum titanate growth.

Paste in $BaTiO_3$ Boule Photo

Figure 4. A boule of cobalt-doped barium titanate grown by the TSSG technique.

4 Poling Barium Titanate

Barium titanate, $BaTiO_3$, is a ferroelectric crystal that is electrooptic, photoconductive and photorefractive [1]. Barium titanate was initially available in the form of thin platelets (~1 mm thick) called "butterfly wings" grown by the Remeika method [2]. Today, boules of $BaTiO_3$ are readily grown by the top-seeded solution growth technique [3] in large size. We typically grow 30-40 gram boules from 400 grams of melt in a 150 cc crucible but, larger boules are easily grown by using larger melts. After crystal growth, samples removed from the boule are multidomain in structure. That is, the sample consists of regions that have their polar axes (spontaneous polarization) oriented orthogonal or antiparallel with respect each other. Multiple domains must be eliminated by aligning the spontaneous polarization everywhere in the sample to create a single domain crystal. The procedure to accomplish this is called poling.

The spontaneous polarization is generated when $BaTiO_3$ makes the structural phase transition from cubic to tetragonal at the Curie temperature of ~130.5 C. It is the displacement of the titanium atoms and a slight displacement of the oxygen and barium atoms from the cubic lattice that gives rise to the polar and ferroelectric nature of the crystal. When cooling through the Curie temperature, the temperature lowering rate, mechanical stresses (external and internal) and thermal gradients will induce 90° and 180° domains as shown in Fig. 1. The spontaneous polarization direction of each domain is indicated by the vectors within that domain.

Each domain is birefringent with ordinary and extraordinary indices of refraction n_o and n_e respectively, where n_e is parallel to the polar direction. In the 90° domains the indices re-orient from domain-to-domain alternating n_e to n_o with a strain induced birefringence at their interface producing a spatial index variation that is easily viewed by the unaided eye. The 180° domains have identical extraordinary indices, n_e, in the opposing directions of polarization (which re-orient on an atomic scale) and the same index n_o in the plane orthogonal to the polarization. The 180°

domains have no observable index variation but can be observed end on when they are preferentially etched and viewed through a polarizing microscope [4].

During the structural phase transformation, phase boundaries propagate across the sample. In $BaTiO_3$ the 90° domains or twins will form because of inelastic stress from a structural misfit at the phase boundary [5]. 180° domains form to maintain electrical neutrality if the phase boundary velocity is too high and the surface charge density too low so that it cannot screen the polarization. In principle, if the phase boundary velocity is low enough, the free carrier concentration high enough and the stress at the phase boundary small enough, a single crystal sample will be formed [5]. In practice these conditions are difficult to achieve and thus alternative approaches to poling have been found.

The discovery of the photorefractive properties of $BaTiO_3$ produced a desire for large volume crystals (> 5 x 5 x 5 mm) that are 100% poled. Currently most of the exciting applications for $BaTiO_3$ are in the field of optical information processing, (e.g self-pumped phase conjugation [6]). Partially poled crystals have diminished photorefractive properties. Indeed, some formulations of the intensity gain coefficient in photorefractive two-beam coupling theory must include a fractional poling factor [7]. In addition, $BaTiO_3$ crystals that are highly conductive are more difficult to pole. We present a technique that optimizes the poling process for high and low conductivity $BaTiO_3$ crystals of large volume and also significantly reduces the sample preparation time and produces high quality $BaTiO_3$.

4.1 Uniaxial Pressing Technique

The elimination of 90° domains can be accomplished by uniaxial pressing on the a-faces of an x-ray oriented sample cut along pseudo cubic {100} crystallographic planes [8]. The dominant orientation of each direction of a multidomain sample can be found by inspecting the crystal between crossed polarizers. After each press many but not all of the 90° domains are generally

eliminated. The pressing of the sample causes internal displacements of atoms which is translated to the surface and produces a surface displacement or "surface steps". The surface steps must be eliminated by polishing before the next pressing of the sample since they mechanically limit or "pin" the displacement of the atoms on the surface. After polishing the six surfaces to eliminate the surface steps the sample is pressed again in the dominant a-axis direction. This process of polishing-pressing often has to be repeated many times and damage to the crystal is highly likely (fracture). It may even lead to pinning of minute internal 90° domains restricted from movement by polishing in a stress. This can produce unwanted scattering centers that are not removed when electrically poled. When the 90° domains are "eliminated" the 180° domains are aligned parallel by heating the sample to near the Curie temperature ~129 C and then applying an electric field greater than the coercive field, E_c~500 V/cm at 129C. Generally the sample is immersed in hot silicon oil to effectively transfer heat to the sample. During electrical poling the sample is illuminated with visible light and viewed between crossed polarizers until the scattered light is minimized. The electrical poling process takes up to eight hours. This mechanical/electrical poling method can take from three to five days to produce a crystal with dimensions 5 x 5 x 5 mm.

4.2 Etching Technique

The basic steps of our etching method to pole $BaTiO_3$ are shown in Fig. 2. The boule is first x-ray oriented and a sample is extracted with a diamond saw from the boule with faces normal to the [100] directions. Typically the 90° domains will be pinned by surface deformations that are induced during the phase transition and from surface damage incurred during cutting and lapping of the sample. To eliminate the saw marks and create a uniform surface for etching, the sample is lapped with 9 μm alumina grit on all sides. Lapping will induce surface microcracks that are approximately twice the grit size [9].

As discussed by Müser et al. [10], a surface with relatively uniform free energy can be created

by etching the sample. In the cubic phase the sample will etch relatively uniformly. Phosphoric acid, H_3PO_4 85%, etches $BaTiO_3$ at 160 C with a rate of ~ 5 μm/min. The samples are etched for one hour. The sample is introduced into the etchant at 125 C from water at 100 C. The etchant temperature is then increased through T_c at a rate of ~ 1-2 C/min to 140-160 C. The sample should be moved periodically to prevent sticking as it's etched. To prevent cracking when etching in a beaker the sample should be supported on a glass platform above the large temperature gradient at the bottom surface of the glass-to-hot plate interface. When cooling, T_c now occurs at a slightly lower temperature ~126 C and a domain phase-front propagates through the crystal that is visually observed. The crystal is then removed and placed in water at ~100 C, this minimizes etching the sample in the polar state where the titanium and oxygen atoms have different etch rates [4] which would further pin the domains. The surface of the sample is relatively "stress free" after the etching process. One may now electrically pole the sample to eliminate 90° and 180° domains choosing any desired crystal face for the **c**-axis. Rytz et al. [11] also poled $BaTiO_3$ without uniaxial pressing. However, they slightly etched their crystals at room temperature. Etching below T_c in the polar state selectively etches the surface and creates surface variations that limit the movement of domains and is not conducive to the elimination of 90 domains.

Ineffective electrical poling and surface cracking can result from space-charge field effects [12] which can lead to a large voltage drop across a small region of the sample near one electrode. When the crystal is heated to ~129 C and a high voltage is applied electrical shorting and cracking are visually observed at one electrode-crystal interface and develop immediately when the high voltage is applied. For hole dominated crystals we find damage at the positive electrode and for electron dominated crystals we find damage at the negative electrode. From the nonuniform space-charge field, potentially all the voltage can be dropped across less than a 1 mm thick region near one electrode. The transverse electrooptic effect was used to observed the electric field distribution across a $BaTiO_3$ crystal. The field strength was spatially nonuniform, it was highest near the positive electrode and reduced in the bulk. This occurs because charge is conducted in the crystal

away from the electrode while charge is not equivalently injected into the crystal from the electrode leaving a charge depletion layer. Shorting occurred at this electrode when the applied field strength was ~1500 V/cm, while weakly illuminated with He-Ne 633 nm laser light. This phenomenon depends on the samples' photo-induced and dark conductivity and nonohmic behavior of the contacts. Thus, the higher the conductivity of the sample the more difficult it will be to electrically align the domains since a major fraction of the applied field will be dropped across a small fraction of the crystal.

To minimize the nonuniform field distribution from photoconductivity electrical poling is done in the dark by enclosing the electrical poling apparatus in a light proof box. The sample is also first dark adapted for one hour to depopulate shallow traps before poling. Dark adaptation and minimizing the duration the voltage is applied helps reduce surface damage and insure complete electrical poling. However, if the dark conductivity is high then dark adaptation is ineffective and the duration over which the field is applied must be minimized by pulsing the applied voltage. Because the surface stress is minimized from etching it is now possible to pulse high voltages across the crystal and induce rapid domain reorientation. Sometimes several short pulses of the voltage are necessary to align the domains. This also reduces piezoelectric induced dimensional changes that could cause 90° domains.

The apparatus used to electrically pole the crystal is shown in Fig. 3. The sample is placed between polished electrodes and immersed in a silicon oil heat bath. With the relatively stress-free condition of the sample and small thermal gradients of the heat bath, the sample can be quickly heated,~ 5 C/min, and stabilized at 129 C where the domains are most mobile. An electrical field (~ 1 kV/cm) is either pulsed or slowly applied, depending on the conductivity of the crystal, that aligns the spontaneous polarization throughout the crystal volume. As one approaches the coercive field a domain phase-front can be seen propagating through the crystal. Immediately thereafter the cooling rate is increased (>2 C/min), the field is turned off and crystal is extracted from the silicon oil at 120 C or could be slowly cooled to room temperature. It should be stressed that the larger

the sample the more one must minimize thermal gradients. (Ideally one should apply electrodes to the sample, bonding wires to the electrodes, and suspend the sample in the oil bath. With this configuration, high dielectric constant oil could be used, (e.g. glycerol), which would minimize fringing field effects.)

After electrical poling, any surface damage at the electrode is removed with 9 μm Al-grit. The crystal is then polished with 3 μm diamond paste. There may be a few 90° domains pinned by the surface but they are usually easily removed by squeezing the crystal between one's fingers along the **a**-axes and by polishing. If their are any 90° domains that remain after polishing they can be easily removed by reheating the sample and applying a short pulse of the field and then repolishing. One can obtain optically flat surfaces by polishing the crystal on aluminum foil (dull side up) which is pressed onto an optical flat (squeezing out the acetone between the two surfaces) and using diamond paste as the polishing compound. The diamond paste is thinned with various solvents depending on the grit size. After final polishing with 0.25 μm diamond paste one should not be able to induce 90° domains by squeezing, indicating a good pole and polish.

Confirmation that one has "completely" poled the sample is accomplished by inspecting the **a**-faces between crossed polarizers which should show a high extinction. In addition, when viewing along the **c**-axis between crossed polarizers one should see an extremely uniform set of color rings and isogyre with a dark cross. Using a He-Ne laser and Glan-Taylor polarizers we measured the extinction ratio along **a** and **c** axes of our crystals and find values typically as high as $\sim 10^{-6}$. And, to confirm that the **c**-face has no 180° domains we etched this surface with HCl. The positive end of the polarization etches faster than the negative end which produces a phase relief of the 180° domains. Inspection under a polarizing microscope typically reveals >99% poling.

In conclusion, we have described a method to pole $BaTiO_3$ that is easily accomplished in less than one working day. The technique leads to high quality single crystals with the desired orientation and of arbitrary dimensions. This process, with appropriate modifications, may

possibly be applied to other ferroelectrics.

References

1. G. C. Valley and J. F. Lam, **61**, 75 (1988).
2. J. P. Remeika, J. Am. Chem. Soc. **76**, 940 (1954).
3. V. Belruss, J. Kalnajs and A. Linz, Mat. Res. Bull. **6**, 899 (1971).
4. J. A. Hooton and W. J. Merz, Phys. Rev. **98** (2), 409 (1955).
5. E. G. Fesenko, V. G. Gavrilyatchenko, A. F. Semenchev and S. M. Yufatova, Ferroel ectrics **63**, 289 (1985).
6. D. J. Pepper, Appl. Phys. Lett **49** (16), 1001, (1986).
7. M. B. Klein and G. C. Valley, J. Appl. Phys. **57** (11), 4901 (1985).
8. P. G. Schunemann, T. M. Pollak, Y. Yang, Y.-Y. Teng and C. Wong, J. Opt. Soc. B **5** (8), 1702 (1988).
9. D. F. Weirauch, J. Electrochemical Soc. **132** (1), 250 (1985).
10. H. E. Müser, W. Kuhn and J. Albers, phys. stat. sol. (a) 49, 51 (1978).
11. D. Rytz, B. A. Wechsler, M. H. Garrett, C. C. Nelson, and R. Schwartz, J. Opt. Soc. Am. B **7** (12), 2245 (1990).
12. V. N. Astratov and A. V. Il'inskii, Ferroelectrics **75**, 251 (1987).

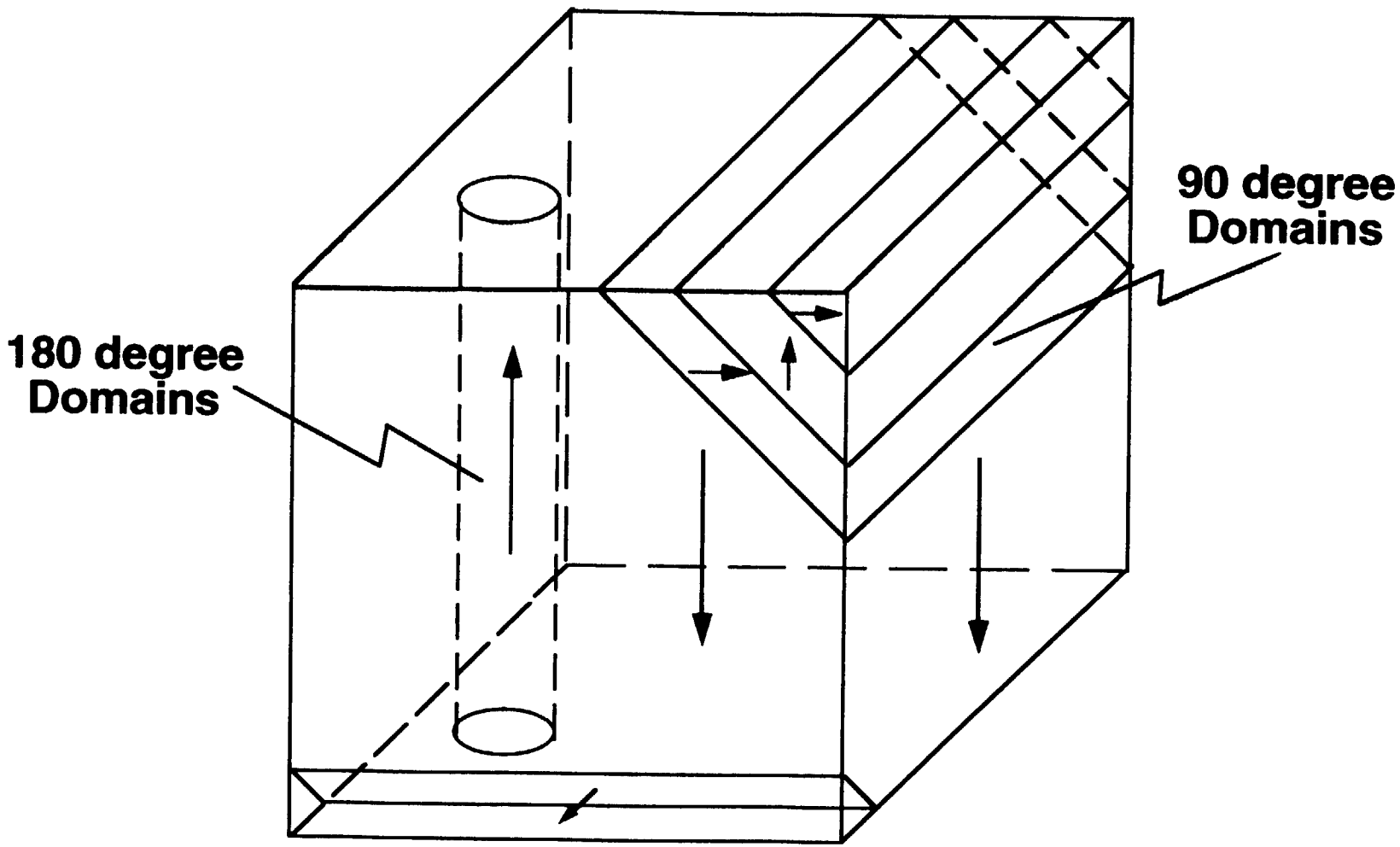

Figure 1. Diagram of the multidomain structure of ferroelectric barium titanate. The vectors show the direction of the spontaneous polarization.

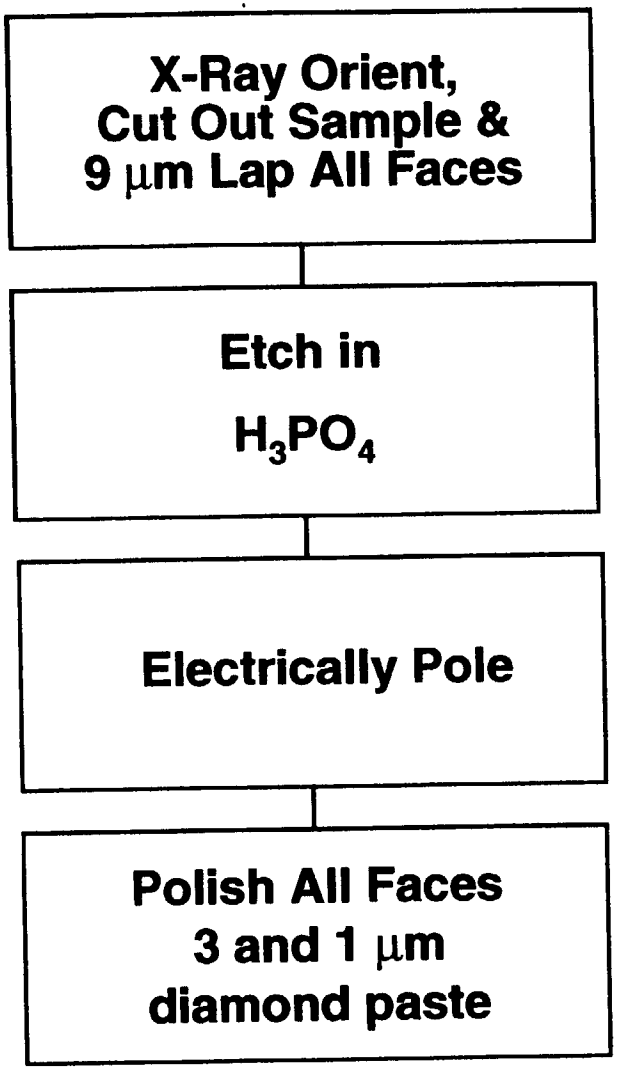

Figure 2. Flow chart of the process developed to produce single-domain barium titanate.

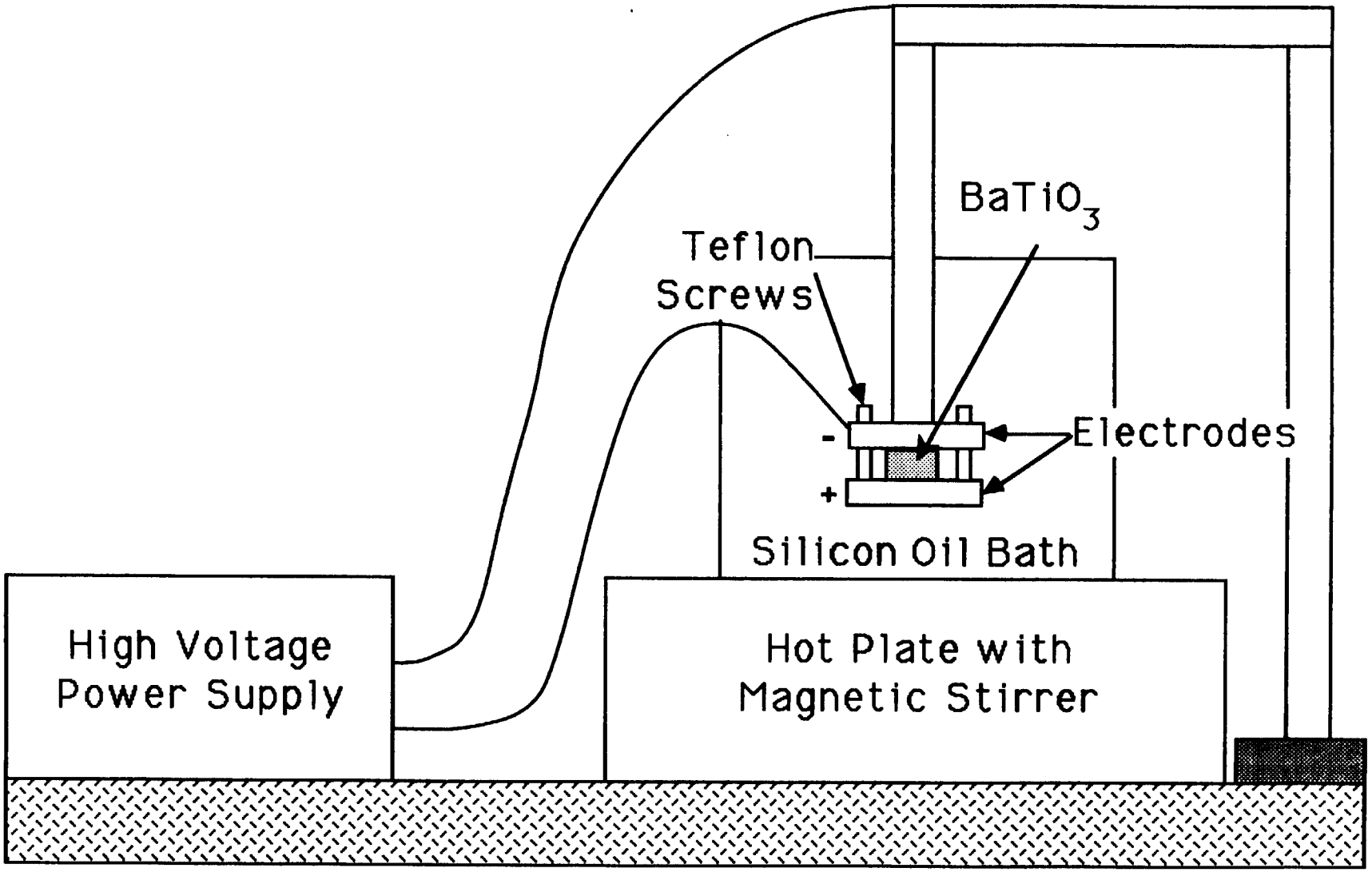

Figure 3. Diagram of the apparatus used to electrically pole barium titanate.

5 The Photorefractive Effect

5.1 The Deep-and-Shallow Trap Model

Consider two coherent plane waves intersecting inside a photorefractive crystal to create a sinusoidal intensity grating with $I(x)=I_o Re[1+m\exp(ik_g x)]$. Photoinduced holes in the valence band diffuse from the bright regions and are trapped in the darker less intense regions creating a sinusoidal charge distribution, and through the linear electrooptic effect produce an index modulation or phase grating that, consistent with Poissons equation, is spatially phase shifted by $\pi/2$ with respect to the intensity interference pattern. This phase shift allows for the coherent diffraction of one beam into the other, producing intensity gain in the signal beam, known as two beam-coupling. A. V. Knyazkov and M. N. Lobanov [1] and Pierce et al. [2] have also described and measured an additive contribution to the gain from absorptive coupling. For beams with ordinary polarization, a grating wavevector $k_g=|\mathbf{k}_2-\mathbf{k}_1|=2\pi/\Lambda_g$ parallel to the c-axis where Λ_g is the grating period and where the pump beam intensity is much greater than the signal intensity to avoid pump depletion the transmitted signal beam intensity I_c is expressed as:

$$I_c(L) = I_0 \exp[(\pm\gamma_{eo} + \gamma_{abs} - \alpha)\, l / \cos\theta], \tag{1}$$

where I_0 is the incident signal beam intensity, θ is internal half angle between signal and pump beam, l is the crystal thickness, α is the absorption coefficient determined at the total intensity of the pump and signal, $\pm\gamma_{eo}$ is the electrooptic contribution to the gain that is dependent on the orientation of the crystallographic c-axis (i.e. the sign of the electrooptic coefficient) and γ_{abs} is the

absorptive coupling.

In the deep-and-shallow trap model, Figure 1, it is assumed that the photoexcited holes not only recombine at the deep traps forming a charge grating, but that charge is also transferred to the shallow level, which may also be absorbing, and thus a shallow level charge grating may also be formed. The strength of this grating depends on the concentration of trapped carriers, M_0, the thermal ionization rate β and the excitation cross-section s_T of the shallow traps. Starting with modified Kukhtarev equations [3], assuming a small intensity modulation, m<<1, and including deep-and-shallow traps in the model Tayebati and Mahgerefteh [4] solved for the first order amplitudes of the space-charge gratings in the deep-and-shallow traps, eN_1 and eM_1 respectively:

$$-eN_1 = -meN_E \frac{k_g^2}{(k_g^2 + k_0^2)} - meM_E \frac{1}{(1 + s_T I_0/\beta)} \frac{k_{0D}^2}{(k_g^2 + k_0^2)}$$

$$eM_1 = -meM_E \frac{1}{(1 + \beta/s_T I_0)} \frac{k_g^2}{(k_g^2 + k_0^2)} + meM_E \frac{1}{(1 + s_T I_0/\beta)} \frac{k_{0D}^2}{(k_g^2 + k_0^2)}, \qquad (2)$$

where e is the charge of the electron, I_0 is the mean intensity, N_E and M_E are the intensity dependent effective deep-and-shallow trap densities, k_g is the grating wavevector, and k_0 is the Debye screening wavevector that is defined by:

$$k_0^2 = k_{0D}^2 + k_{0T}^2, \qquad (3)$$

where k_{0D} and k_{0T} are the deep-and-shallow trap screening wavevectors that are proportional to square root of the deep-and-shallow effective trap densities. From Poisson's equation the space-charge induces a space-charge field, $E_1 = -(ie/k_g \varepsilon \varepsilon_0)(N_1 - M_1)$, where:

$$E_1 = -im\frac{k_B T}{e}\frac{k}{1+k^2/k_0^2}\eta(I), \tag{4}$$

and

$$\eta(I)=\frac{1}{k_0^2}\left[k_{0D}^2+\frac{k_{0T}^2}{1+\beta/s_T I_0}\right]. \tag{5}$$

Here $\eta(I)$ is the intensity dependent factor with $0<\eta(I)\leq 1$, k_B is Boltzmann's constant, and T is the absolute temperature. The electrooptic gain is given by $\gamma_{eo}=i(2\pi r_{eff}/nm\lambda)E_1$ where $r_{eff}=n^4 r_{13}$ for ordinary polarization and the electrooptic coefficient equal to $r_{13}=19.5$ pm/V, and n is ordinary index of refraction equal to 2.488 at $\lambda=514.5$ nm. The space-charge field of eqn. (4) is similar in form to that of the Kukhtarev model but also includes intensity dependence expressed in $\eta(I)$ and effective deep-and-shallow trap densities are also intensity dependent.

Absorption gratings have been measured by Pierce et al. [2] and Cudney et al. [5] in a geometry that has no electrooptic gain. The absorptive coupling arises because of the spatial variation in charge density in both the deep-and-shallow levels where the absorptive gain is given as [4]:

$$\gamma_{abs} = \frac{\hbar\omega}{m}\left(s_D N_1 - s_T M_1\right). \tag{6}$$

In the limit of small k_g from eqn. (3) $N_1=M_1$ and the absorptive gain is proportional to $(s_D-s_T)N_1$ which predicts for $s_T > s_D$, (which will give light-induced absorption), that $\gamma_{abs} < 0$, i.e. negative absorptive screening gratings or a negative "offset" as called by Cudney et al. [5]. On the other

hand when $s_T < s_D$ one will find light-induced transparency and positive absorptive coupling. This is typical of the reduced samples we produced that are n-type photoconductors.

5.1.1 Beam-Coupling Measurement Technique

To determine the electrooptic and absorptive gain coefficients we measured the effective gain, γ_0, for the ± c-axis orientations of the crystal with a pump to signal ration of r=800:1 using the experimental set up shown in Figure 2. Motes and Kim [6] also made this measurement but they did not determine an absorptive contribution to the gain. They measured light-induced absorption whereas we eliminated intensity dependent absorption from our measurement by using the method introduced by Pierce et al. [2] in which the effective gain is determined from two measurements: (a) the pump beam coherent with the signal beam and, (b) the pump beam incoherent with the signal beam. That is,

$$\gamma_0^{\pm} \equiv \frac{I_c(L)}{I_{inc}(L)} = \frac{I_s \text{ with Coherent pump}}{I_s \text{ with Incoherent pump}}$$

$$= \frac{I_0 \exp\{[\pm\gamma_{eo} + \gamma_{abs} - \alpha]\, l / \cos\theta\}}{I_0\{\exp[-\alpha]\, l / \cos\theta\}}$$

$$= \exp\{[\pm\gamma_{eo} + \gamma_{abs}]\, l / \cos\theta\} \quad . \qquad (7)$$

The pump beam was made incoherent with the signal by rapidly vibrating a mirror at rate and amplitude that was faster than the grating formation time then measuring I_{inc}. The vibration was then stopped so that the signal beam experienced beam-coupling and this measurement resulted in I_c. In this way the pump beam continuously illuminates the crystal so that the absorption is the same when determining the signal transmission, and is therefore eliminated in the ratio of I_c/I_{inc}. Coherent scatter into the signal direction was eliminated by a method similar to Pierce et al. [2], and the signal beam was focused through a pin hole to spatially filter other noise components.

Coupling due to the back reflections into the coupling region was minimized by placing the crystal in an oil-filled cuvette that reduced the back surface reflectivity to ~6%.

The electrooptic and absorptive components of the gain were then determined by measuring the effective gain for signal amplification, γ^+, and then gain for signal depletion, γ-, by simply exchanging the roles of the signal and pump by changing their relative intensities. In this way the effective gain is determined in two orientations where the absorptive component does not change sign. The net effective gain for these two measurements is given as,

$$\gamma^{\pm} \equiv (\pm\gamma_{eo} + \gamma_{abs}) = \frac{\cos(\theta)}{l} \ln[\gamma_0{}^{\pm}] . \tag{8}$$

The electrooptic and absorptive gain is then determined by one-half of the difference or sum of the net gain coefficient:

$$\gamma_{eo} = \frac{\gamma^+ + \gamma^-}{2} \quad \text{and} \quad \gamma_{abs} = \frac{\gamma^+ - \gamma^-}{2} . \tag{9}$$

We note that from the direction of the beam-coupling with respect to the direction of the positive c-axis the majority carriers can be determined.

References

1. A. V. Knyazkov and M. N. Lobanov, Sov. Tech. Phys. Lett. **11**, 365 (1985).

2. R. M. Pierce, R. M. Cudney, G. D. Bacher and J. Feinberg, Opt. Lett. **15**, 414 (1990).P.

3. V. Kukhtarev, V. B. Markov, S. G. Odoulov, M. S. Soskin and V. L. Vinetskii, Ferroel ectrics **22**, 949 (1979).

4. Tayebati and D. Margerefteh, J. Opt. Soc. Am. B 8(**5**), 1053 (1991).N.

5. R. S. Cudney, R. M. Pierce, G. D. Bacher, and J. Feinberg, J. Opt. Soc. B 8(**6**), 1326 (1991).

6. A. Motes and J. J. Kim, Opt. Lett. **12**, 199 (1987).

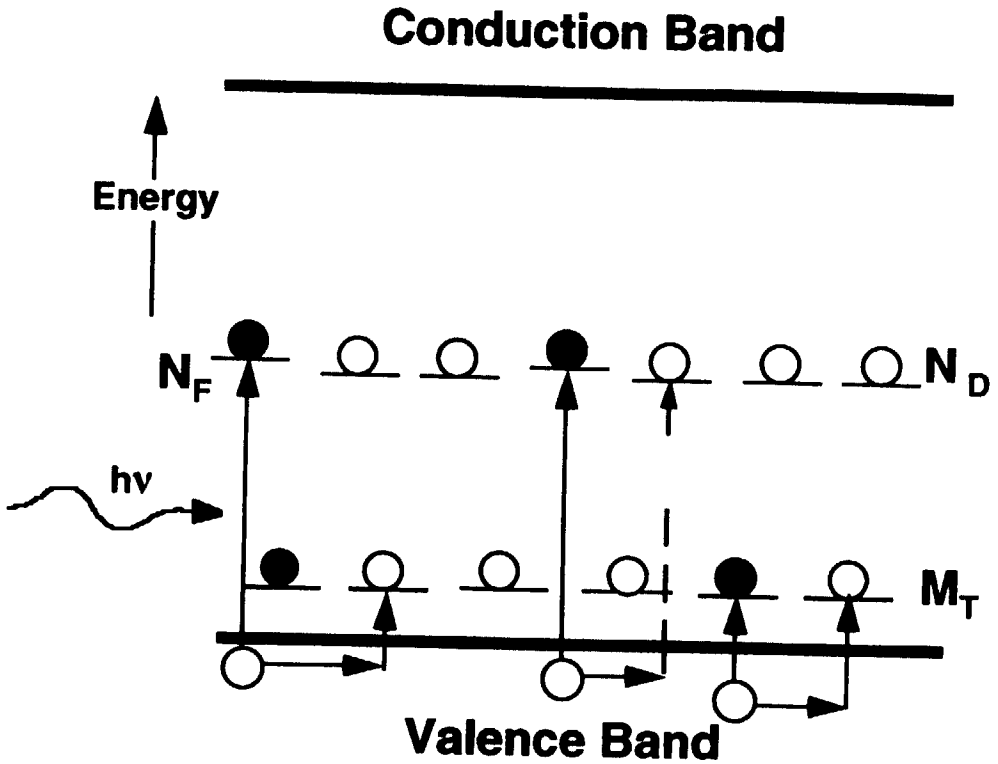

$$\alpha(I)=h\nu[s_D N_{DF}+(s_T-s_D)M_0]$$

N_D is the Deep Trap Density
M_T is the Shallow Trap Density
N_F is the Uncompensated Deep Trap Density

Figure 1. Deep-and-shallow trap energy level model used to describe the photorefractive effect in barium titanate. Holes may be photoexcited from deep levels N_{DF} and shallow levels M_T into the valence band and recombine to deep or shallow traps. The absorption is from the deep traps, $h\nu s_D N_{DF}$, and the shallow level, $h\nu s_T M_0$, and the absorption diminishes in the amount transfered to the shallow level, $-h\nu s_D M_0$. If $s_T > s_D$ then there will be light-induced absorption. If $s_T < s_D$ then there will be light-induced transparency.

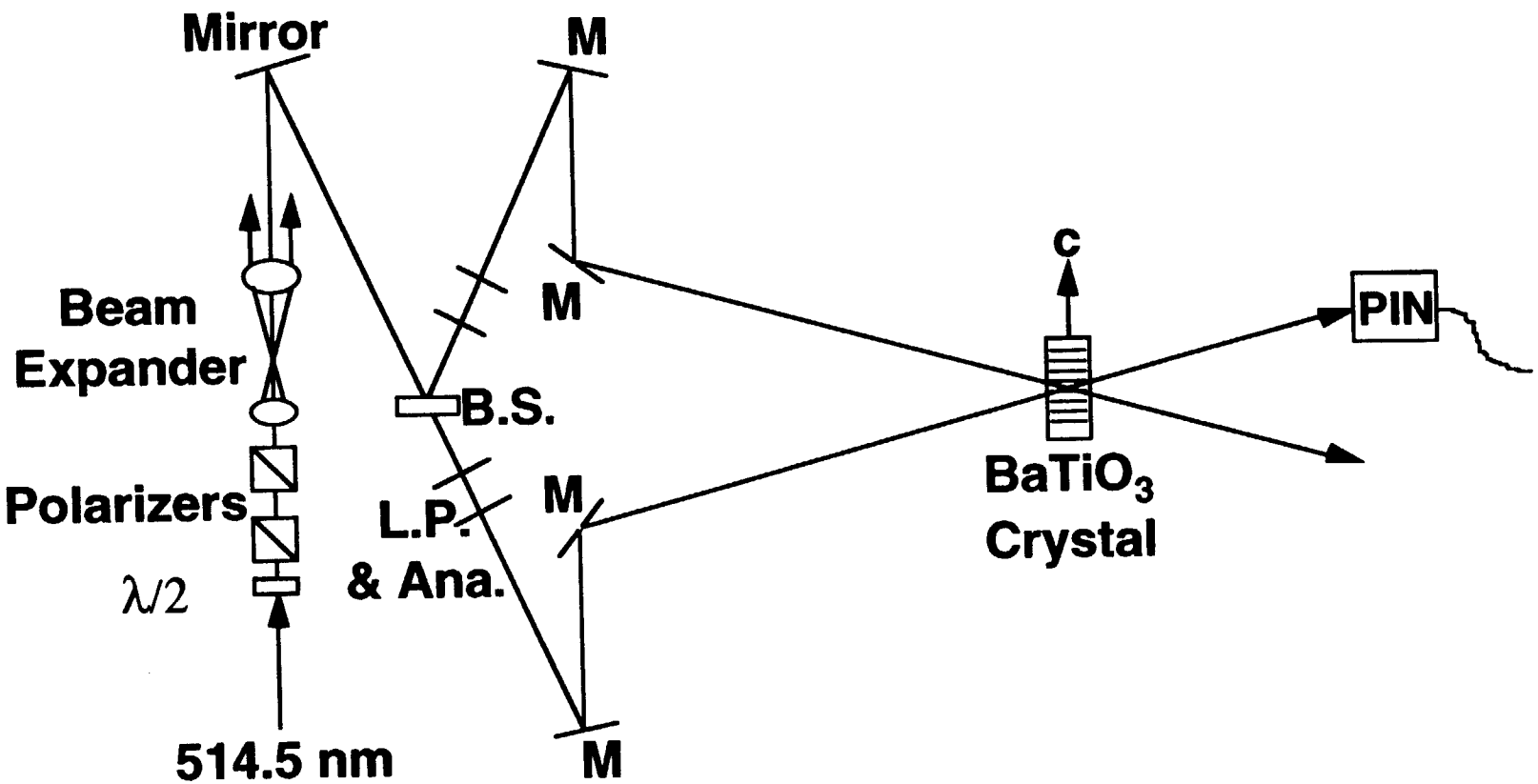

Figure 2. Diagram of the experimental set up used to characterize the photorefactive properties of barium titanate. B. S.=beam splitter, L.P.=linear polarizer, Ana.=analyzer, M=mirror, λ/2=half-wave plate.

6 Oxygen-Reduction of Barium Titanate

The effect of oxygen-reduction of barium titanate on its photorefractive properties was first investigated by Ducharme and Feinberg [1] who found a slight increase in beam-coupling and decrease in response time with reduction to 10^{-5} atm. Wechsler et al. [2] reported similar results over a wider range of partial pressures and noted a tenfold decrease in the response time to 100 msec at partial pressure $P_{O2}=10^{-12.2}$ atm. Schunemann, Temple et al. [3] studied the effect of oxidation and reduction and Schunemann, Pollak et al. [4] characterized the photorefractive properties of barium titanate as a function of the feed materials and reduction state. In particular, the latter found that when they heavily reduced their nominally undoped samples in 1% CO/CO_2 or 10% CO/CO_2, ($P_{O2}<10^{-11}$ atm), that they had a then fold increase in the gain and thus sensitivity at 633 nm. One unique feature in the absorption spectra of these samples is an absorption peak at ~450 nm. Described herein is our investigation of the dependence of the photorefractive effect on the reduction state. We have found that the absorption peak at 450 nm can be induced with nominally undoped barium titanate, crystals grown from purified source materials or even with doped samples ([Co]=20 ppm). Since the reduction level is in the intrinsic regime as discussed in section 2 on defect chemistry and, the absorption feature appears to be independent of the impurity concentration we propose that the absorption feature at 450 nm is associated with an intrinsic defect induced by oxygen vacancies. We will show in section 8 that the photorefractive gain in the reduced sample is equivalent to the as-grown cobalt-doped crystal but the response time is reduced by a factor of three, measured at 514.5 nm. We note that the gain of the samples prepared by Schunemann et al. [4] was very low which may be because they used 633 nm illumination for characterization and that the heavily reduce samples have high dark conductivity making them more difficult to pole.

Five 20 ppm cobalt-doped samples were extracted from the same boule. The samples were

heavily reduced by using the 10% CO/CO_2 purified gas, annealing at different temperatures to get the oxygen partial pressure between 10^{-12} atm at 800 C, and 10^{-17} atm at 1000 C. Equilibrium times at each temperature were determined by computing the annealing duration from,

$$t=(\frac{l^2}{\pi^2 D})\ln(\frac{4C_0}{\pi C}), \quad (1)$$

where l is the sample thickness (cm), C is the concentrations at the center of the sample, C_0 the initial concentration at the surface ($C_0/C=100$ for 99% equilibration), and D is the bulk diffusion coefficient of oxygen vacancies in barium titanate. The diffusion coefficient is given by Wernicke in [5] as,

$$D=5700\exp(-2.05eV/kT)\ cm^2/s. \quad (2)$$

Samples were then quenched to room temperature to preserve the oxygen vacancies in the reduced state. The quenching time from high temperature to 200 C was three to five minutes. The annealing temperatures are shown in Figure 1.

From Figure 6 in section 2.2 on defect chemistry, the turn-over for a barium titanate crystal, which has ~500 ppm background acceptors, from the extrinsic to the intrinsic state conduction state is at the oxygen partial pressure of 10^{-10} atm at 1000 C. The turn-over point increases with lower doping levels and also decreases with an increase in the annealing temperature (for 800 C the turn-over is at ~10^{-15} atm). This implies that the annealing conditions are all in or near the intrinsic regime, i.e. the properties are controlled by the oxygen vacancies and electrons. These five reduced crystals have n-type electrical conductivity while the as-grown has p-type electrical conductivity.

Shown in Figure 1 are the optical absorption spectra measured using a Perkin-Elmer λ–9

spectrophotometer determined between 350 and 860 nm with the field perpendicular to c-axis. The undoped crystal grown from purified feed is given as a reference spectra. Cobalt-doping in barium titanate causes an absorption that extends from band edge throughout the visible range. The effect of reduction can be separated two parts: (1) increasing the absorption at the peak at ~450 nm in all reduced crystals; (2) decreasing absorption from 550 nm to 800 nm for two reduced crystals while increasing absorption for the other two crystals. The exact partial pressure is unknown since we varied the temperature of the reduction. However, the increase in absorption of sample number 6 is probably due to the increase in free carrier absorption. This implies that this is the most heavily reduced sample. In fact, measurements of its high dark conductivity ($<10^{-9}$ $\cdot\Omega$-cm^{-1}) also indicate that it is the most heavily reduced sample. Thus, decreasing the temperature while keeping the input CO/CO_2 ratio constant lowers the reduction level. This lowers the free carrier absorption and the absorption in the visible decreases in the sequence 6,5,4,3. However, when the temperature is at 810 C the absorption peak at 450 nm clearly appears and the absorption diminishes into the visible and near infrared.

Essentially, reduction allows one to alter the position of the Fermi level changing the dominant carrier type from holes to electrons. Reduction of $BaTiO_3$ produces singly and doubly ionized oxygen vacancies which are shallow traps just below the bottom of the conduction band and are responsible for an increase in dark conductivity. That is, shallow traps by definition have wavefunctions that are spread over many unit cells. The weakly bound electrons resulting from the oxygen vacancies can be transferred to the transition metal ion impurities and the latter will therefore be reduced, e.g. $[Co^{3+}]+e \dashrightarrow [Co^{2+}]$. Thus, the number of Co^{3+} sites for carrier recombination has diminished. We have found from conductivity measurements of cobalt-doped barium titanate in the as-grown state that the higher the cobalt concentration the lower the dark conductivity and photorefractive sensitivity. This suggests that cobalt in the 3+ valence state is a strong recombination center and thus responsible for short free carrier lifetimes in the as-grown cobalt-doped crystals. However, when these crystals are reduced there is a diminished

concentration of this valence state and the free carrier lifetime could possibly increase since the free carrier lifetime is inversely proportional to the concentration of recombination centers and their recombination rate coefficient as will expanded upon in section 6.

References

1. S. Ducharme and J. Feinberg, J. Opt. Soc. Am. B **3**, 283-293 (1986).

2. B. A. Wechsler, M. B. Klein, and D. Rytz, *Lasers and Nonlinear Optical Materials*, L. G. DeShazer, ed., Proc. Soc. Photo-Opt. Instrum. Eng. **681**,91 (1986).

3. P. G. Schunemann, D. A. Temple, R. S. Hathcock, C. Warde, H. L. Tuller, and H. P. Jenssen, *Digest of Topical Meeting on Photorefractive Materials, Effects, and Devices* (Optical Society of America, Washington, D.C., 1987).

4. P. G. Schunemann, T. M. Pollak, Y. Yang, Y.-Y. Teng, and C. Wong, J. Opt. Soc. Am. B **5**, 1702 (1988).

5. R. Wernicke, Philips Res. Rpts. **31**, 526 (1976).

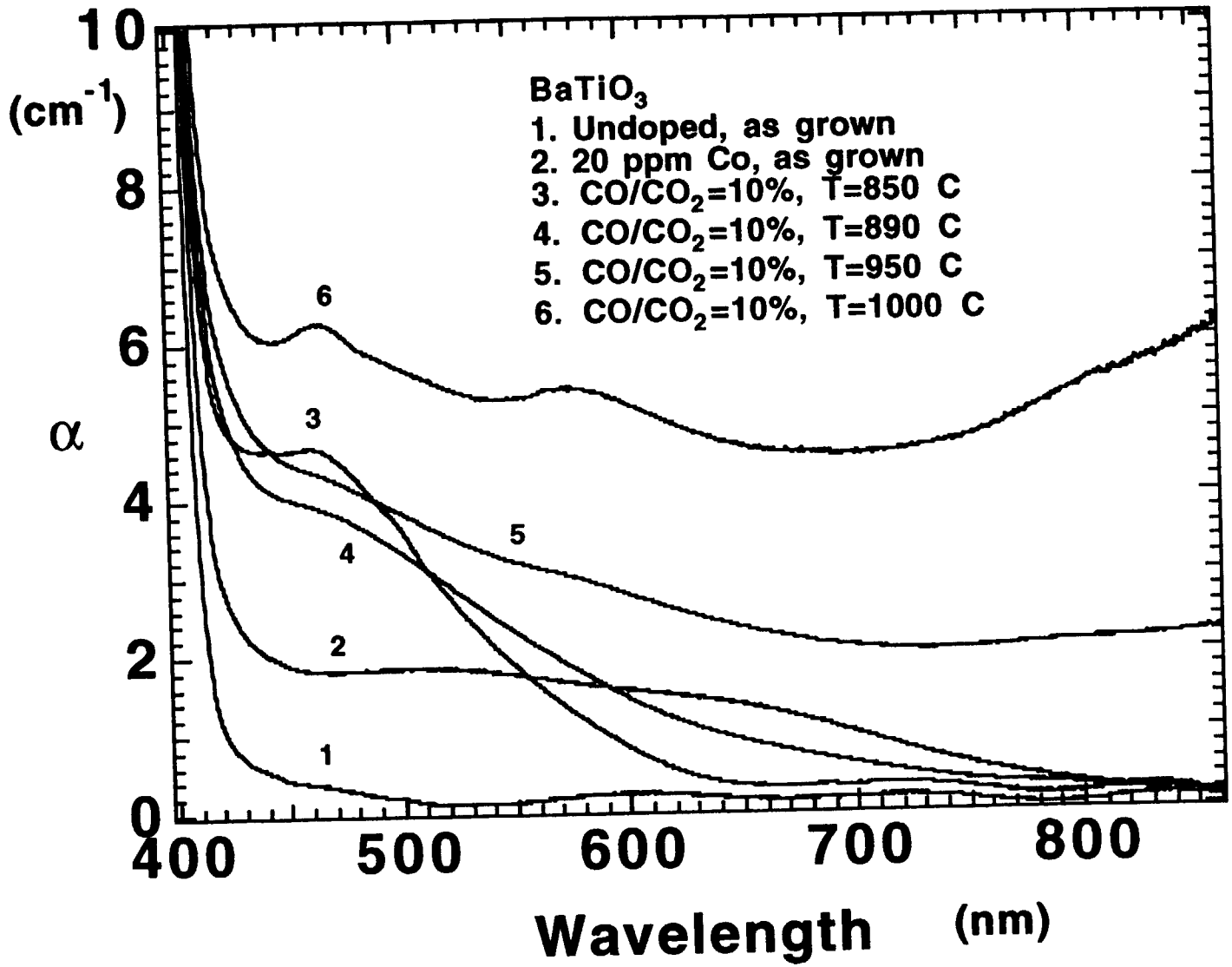

Figure 1. Absorption spectra of nominally undoped $BaTiO_3$ grown from purified source materials, five samples (No.'s 2-6) of 20 ppm cobalt-doped barium titanate and with different reduction conditions.

7 Photorefractive Properties of Reduced Barium Titanate

7.1 Beam-Coupling Measurements

Barium titanate, $BaTiO_3$, has the largest known third-rank electrooptic tensor component of inorganic crystals, r_{42}=1640 pm/V [1]; this leads to high beam-coupling gain without applied fields, but the response time of the material is usually slow, e.g. 1 sec at 1 W/cm^2. However, we have improved the response time of as-grown cobalt-doped barium titanate by a factor of ~4.5 through oxygen-reduction while maintaining the beam-coupling gain. In addition, in the 45°-cut orientation where the crystal is cut at 45° with respect to the **c**-axis (see Fig. 1), which then allows one to easily utilize the r_{42} electrooptic coefficient in beam-coupling, we find that the response time is comparable to that of a 0°-cut for a sample from the same n-type $BaTiO_3$ crystal. The higher gain in the 45°-cut (38.7 cm^{-1}) and equivalent response time lead to a photorefractive sensitivity that is 3.44 cm^3/kJ. This is, to the best of our knowledge, the highest reported to date for $BaTiO_3$. In addition, to the best of our knowledge it is also higher than that reported for reduced potassium niobate [2], ($KNbO_3$:Fe), or strontium barium niobate chromium-doped [3], (SBN:60:Cr), but slightly less than bismuth silicon oxide [4], (BSO).

For $BaTiO_3$ in the 0°-cut orientation (a 0°-cut has crystal faces normal to the **a** and **c**-axes) it is difficult for beam-coupling experiments to access the r_{42} electrooptic coefficient except at steep entrance angles. To exploit the higher electrooptic coefficient and thus produce high beam-coupling gain, Ford et al. [5] proposed and demonstrated that by using a 45°-cut $BaTiO_3$ crystal they could obtain a beam-coupling gain of 26 cm^{-1}. Ford et al. also measured a faster beam-coupling response time in the 45°-cut with respect to the 0°-cut but with two crystals from different boules. Pepper [6] found that the self-pumped phase conjugate rise time for two crystals, 0° and 45°-cut, from the same boule was faster by a factor of ~3 and the self-pumped phase

conjugate reflectivity increased by 12%. In addition, it was reported by Ewbank et al. [7] that in a wedged sample of $BaTiO_3$, where the r_{42} electrooptic coefficient could be accessed and the interaction length could be altered, that gains as high as 65 cm^{-1} were obtained when the sample thickness was approximately 1 mm or less, (with pump depletion from beam fanning minimized).

We have made beam-coupling and response time measurements on the same cobalt-doped oxygen-reduced crystal initially in the 0°-cut and then sectioned into a thin (0.870 mm) 45°-cut sample. Our comparison of these two orientations described herein shows that the gain is indeed increased in the 45°-cut with respect to the 0°-cut but one also obtains a nearly equivalent response times leading to a higher photorefractive sensitivity in the 45°-cut crystal.

The functional dependence of the electrooptic gain coefficient including effects of deep-and-shallow traps is given in the following expression [8],

$$\gamma = \frac{2\pi n^3}{\cos\theta_i}\frac{k_B T}{e}\frac{r_{eff}}{\lambda}\left(\frac{k_g}{1+k_g^2/k_0^2}\right)\eta(I)(e_1\cdot e_2^*) \quad . \tag{1}$$

Here, n is the appropriate index of refraction, r_{eff} is the effective electrooptic coefficient, $k_B T$ is Boltzmann's constant times the absolute temperature, e is the magnitude of the electron charge, k_g is the grating wavevector, k_0 is the Debye screening wavevector, e_1 and e_2 are the unit polarization vectors, θ_i is the internal half-angle, and $\eta(I)$ is an intensity dependent factor where $0 \le \eta(I) \le 1$.

The effective electrooptic coefficient for the 0-°cut crystal using ordinary polarization is given in [9], as

$$r_{eff} = n_o^4 r_{13} \sin(\theta_i), \tag{2}$$

where n_o is the ordinary index of refraction, r_{13} is the contracted third rank electrooptic tensor

component. In a 45°-cut sample the normal to the entrance face is at 45° with respect to the c-axis and for beams that are bisected by the normal, the grating wavevector is at 45° with respect to the c-axis (see Figure 1). For the 45°-cut the effective electrooptic coefficient for extraordinary polarization is given in [9] as,

$$r_{eff} = \frac{1}{n^4}\{n_o^4 r_{13}[\cos 2\theta_i - \cos 2\beta] + 4n_e^2 n_o^2 r_{42}\sin^2\beta + n_e^4 r_{33}[\cos 2\theta_i + \cos 2\beta]\}\cos 2\beta \quad . \tag{3}$$

The indices of refraction are n_o=2.488 and n_e=2.424, and electrooptic coefficients are r_{13}=19.5 pm/V, r_{33}=97 pm/V [10] and r_{42}=1640 pm/V. The internal angles for beams whose bisector is normal to the entrance face are determined from Snells law and by transforming the index of refraction using the equation for the index ellipsoid (resulting in a transcendental equation) where we will give the experimental and theoretical values of the gain using an external half-angle between the beams of 25.4 degrees.

The Debye screening wavevector, k_0, is inversely proportional to the square root of the dc dielectric constant. The magnitude of the dc dielectric constant in the direction of the grating wavevector is determined by the transformation, $\varepsilon = \hat{k}_g \cdot \vec{\varepsilon} \cdot \hat{k}_g$, where $\vec{\varepsilon}$ is the relative dc dielectric tensor with components $\varepsilon_{11}=\varepsilon_{22}=3600$ and $\varepsilon_{33}=150$ [11] and $\hat{k}_g$ is the normalized grating wavevector. Shown in Figure 2 is a plot of the dc dielectric constant as a function of the angle between the grating wavevector and the c axis. (For an angle of 45° the dc dielectric constant is equal to 1875.)

As shown in Figure 3 there is a peak in the beam-coupling gain for an internal beam-crossing angle of ~ 6° and an angle between the c axis and the grating wavevector of β~45° when the

changes in the effective electrooptic coefficient for extraordinary polarization, the Debye screening wavevector, and the grating wavevector as a function of the internal half-angle between the beams and the angle between the grating wavevector and the c axis are incorporated into equation (1).

To determine the photorefractive properties of a 0° and 45°-cut $BaTiO_3$ crystal we first grew a cobalt-doped 20 ppm (parts per million, in the melt) barium titanate boule by the top-seeded solution growth technique. (Cobalt-doping is know to enhance the gain.) An x-ray oriented 0°-cut sample was extracted from the boule. This sample was fabricated into a single-domain crystal with an etching and electrical poling technique [12]. It was polished to an optical quality finish with dimensions 6.90 mm x 5.16 mm x 4.52 mm where the **c**-axis was parallel to the long dimension. The crystal was then oxygen-reduced, $P_{O2}=10^{-15}$ atm, to obtain n-type barium titanate (confirmed by the direction of beam-coupling with respect to the polar axis) that had an absorption coefficient at 514.5 nm of 2.2 cm^{-1} (measured at the intensity of the beam-coupling measurements). The sample had an intensity-induced change in absorption of $\Delta\alpha=-1$ cm^{-1} (light-induced transparency). The crystals absorption spectra at low intensities and the difference spectra between the undoped crystal and the reduce crystal are shown in Figure 4. A distinct absorption peak located near the band edge (460-490 nm) is characteristic of $BaTiO_3$:Co crystals that are heavily reduced. As pointed out in the section on defect chemistry this absorption peak is probably associated with an intrinsic defect.

Beam-coupling and response time measurements were made with the 0°-cut crystal placed in a cuvette filled with silicon oil. To obtain an accurate measurement of the gain in the 0°-cut (avoiding beam fanning effects) we used argon ion laser illumination at 515.5 nm that was ordinary polarized and the grating wavevector was parallel to the **c**-axis thus accessing the smallest electrooptic coefficient r_{13}. The pump beam was expanded to a diameter of 2 cm, completely enveloped the 1 mm diameter signal, and the former had an intensity of 1 W/cm^2. The pump-to-signal ratio was 800:1 to avoid pump depletion. Shown in Figure 5 is the gain as a function of intensity for the as-

grown and reduced cobalt doped crystals. We note that at 1 W/cm^2 the gain is equivalent in the two crystals but the response time has decreased by a factor or ~4.5. For the 0°-cut reduced crystal the Debye screening wavevector was determined to be $k_0(0°)=1.76 \times 10^7$ m^{-1} and the intensity dependent factor $\eta(I)=0.51$. These values along with the computed effective electrooptic coefficients were used to predict the gain for other crystallographic cuts and light polarizations.

The 0°-cut sample was then sectioned into a 45°-cut crystal and optically polished with an orientation as shown in Figure 1. The crystal had a thickness of 0.870 mm and a cross-section of 5 mm^2. With this thickness the reduction of the gain from beam fanning and thus pump depletion should be negligeable [7]. Beam-coupling measurements were then made with extraordinary and also ordinary polarization and the bisector of the grating writing beams was normal to the entrance face making the grating wavevector at 45° with respect to the c-axis.

Shown in Table 1 are the computed effective electrooptic coefficients, predicted and observed beam-coupling gain coefficients and the intensity beam ratios used when measuring these values. First we note that it is difficult to make a good measurement of the 45°-cut crystal's gain when using ordinary polarization since any extraordinary component will strongly influence the gain because of the large r_{42} electrooptic coefficient. Second, we found that there was a large amount of fanning when using extraordinary polarization producing low signal to noise giving a large uncertainty in the measured gain coefficients. In addition, when we reduced the beam ratio from 10^5 to 10^4 the gain did not change within our experimental error and thus it may be possible that fanning gratings were slightly depleting the pump beam.

Another reason for the discrepancy in the magnitudes of the gain shown in Table 1 may be due to incorrect values of the unclamped electrooptic coefficients since these were not measured for our crystal but taken from the literature. In addition, it was recently reported by Zgonik and Günter [13] that neither the unclamped (used here) nor the clamped values of the electrooptic coefficients should be used to calculate the effective electrooptic coefficient since the space-charge field is not

equivalently unclamped in all directions. The magnitudes of the electrooptic coefficients (and thus the effective electrooptic coefficients) are dependent on the crystallographic orientation with respect to the grating wavevector and are smaller than the unclamped values which would lead to a lower value of the gain.

The gain dependence on grating wavevector for the 45°-cut crystal was determined using extraordinary polarization and is shown in Figure 6. The peak in the gain coefficient ~38.7, within our experimental error, is comparable to that predicted by equation (1) and shown in Figure 3. From the beam-coupling data for the 45°-cut shown in Figure 4 we determined from the best fit curve that the peak of the gain for the 45°-cut to be at a grating period of ~1.17 μm. From equation (5) one predicts the Debye screening length, $(2\pi/k_0)$, of the 45°-cut to be equal to ~1.2 μm as compared with our best fit experimental value of ~1.17 μm.

7.2 Response Time Measurements

Shown in Figure 7 is the diffraction efficiency of a He-Ne readout beam as a function of time when the grating is erased by a beam of 1 W/cm^2 and when the beam ratio was 24:1. With this writing beam ratio, which satisfies the small modulation approximation [14], the diffracted probe will still accurately represent the time evolution of the space-charge field. The 1/e decay time or response time is approximately ~21 msec for the 45°-cut crystal and ~34 msec for the 0°-cut crystal. As previously noted oxygen-reduction lowered the response time by a factor of ~4.5 for this $BaTiO_3$:Co sample, although we have measured even faster response times in other reduced $BaTiO_3$ crystals.

In Figure 8 is the response time as a function of intensity for the two crystallographic cuts. One can see that the response times are nearly equivalent. A formulation for the response time, τ, [15], not including a grating wavevector dependence, shows that τ is directly proportional to the dc dielectric constant and inversely proportional to the mobility-lifetime product $\mu\tau_r$ and excitation cross-section s, i.e.,

$$\tau \propto \frac{\varepsilon\varepsilon_0}{\mu\tau_r s}. \tag{5}$$

From this formulation one might expect that the response time would increase in the 45°-cut orientation in proportion to the increase in the dc dielectric constant. Since the dc dielectric constant has increased from 150 in the 0°-cut crystal to 1875 in the 45°-cut orientation the mobility-lifetime product must also be increasing with an equivalent percentage change to obtain nearly equivalent response times. And, since we have examined the same crystal the lifetime should be approximately the same for the two crystallographic cuts. This means that the mobility scales with

the dc dielectric constant. Since the dc dielectric constant follows changes in the lattice as does the phonon density this implies that the mobility is phonon limited (not trap limited) in barium titanate. Mahgerefteh et al. [16] also recently reported this same conclusion. It is important to realize that the anisotropy of the dielectric constant and mobility product in this n-type perovskite with an ABO_3 lattice in the tetragonal phase, vary in the same manner with reorientation. And, in the expression for the response time they are in a ratio which permits the response time to remain constant with reorientation while accessing the larger electrooptic coefficient.

The tensor components of the mobility for holes, (photorefractively determined [17]), assuming a equal free carrier lifetime of 1 nsec are, $\mu_{11}= \mu_{22}=7.35$ cm^2/V-sec and $\mu_{33}=0.44$ cm^2/V-sec. (Note, if the free carrier lifetime is 0.1 nsec the mobilities increase by an order of magnitude.) The anisotropy of the mobility of electrons was measured using the Hall-effect by Berglund and Baer [18]. At 26 C they determined the tensor components of the mobility to be: $\mu_{11}=\mu_{22}=1.2$ cm^2/V-sec and $\mu_{33}=0.13$ cm^2/V-sec [18]. (These latter measurements were performed on highly conducting $BaTiO_3$.) The mobility transforms as $\mu = \hat{k}_g \cdot \vec{\mu} \cdot \hat{k}_g$ and has the angular dependence as shown in Figure 9. Here we have inferred that the ratio of the dc dielectric constant to the mobility is constant (150) and thus arbitrarily assign the mobility a value of 1 cm^2/V-sec for μ_{33} and 24 cm^2/V-sec for μ_{11} and μ_{22}.

Including the effects of the inverse diffusion length K, Debye screening wavevector k_o and grating wavevector k_g the response time t has the following formulation,

$$t = \frac{\varepsilon_o \varepsilon_r}{qn\mu}\left[\frac{1+k_g^2/K^2}{1+k_g^2/k_o^2}\right]. \qquad (6)$$

Where, the inverse diffusion length $K^2=(\mu\tau_f k_B T/e)$ and n is the number density of photoexcited

electrons which is proportional to the free carrier lifetime τ_f and the quantum efficiency. Usually in $BaTiO_3$ the inverse diffusion length is on the order of 25 μm^{-1} which is much larger than the grating wavevector and thus the second term in the numerator in the brackets of equation (6) is neglected. This is primarily because the free carrier lifetime is very small, on the order of 100 psec or less [19].

Shown in Figure 10 is a plot of equation (6) for two values of the free carrier lifetime and as a function of the internal beam's crossing half-angle and for different crystallographic cuts which alter the dc dielectric constant (Figure 2) seen by the space-charge field. In addition, we have include the anisotropy of the mobility as shown in Figure 9. Changes in the coefficient before the square brackets simply scale the response time. We note that with a free carrier lifetime of 100 psec the inverse diffusion length is still much larger than the grating wavevector ($K>>k_g$) even when we incorporated the anisotropy of mobility and thus one may neglect the second term of the numerator as previously stated. The lower curves correspond to these conditions and are controlled by the anisotropy of the dc dielectric constant. This predicts that for an internal beam crossing angle of ~10 degrees, as we have examined, that the response times of the 0° and 45° -cut crystals should differ by ~3.5. As can be seen from Figure 8 the response times are nearly equivalent. If the free carrier lifetime is increased to 2.5 nsec (a factor of 25) this gives the upper set of curves and the difference in response times between the crystallographic cuts diminishes and more closely coincides with our nearly equivalent response times. If the free carrier lifetime is increased further to ~5 nsec the curves will coalesce and have little difference in response time between the response times of the 0° and 45° crystallographic cuts as we observe experimentally. In addition, this also predicts that the response time should be nearly equivalent as a function of beam-crossing angle or grating wavevector. Shown in Figure 11 is a plot of the response time as a function of grating wavevector for an erase intensity of 250 mW/cm^2 for a cobalt-doped oxygen reduced $BaTiO_3$ crystal. As one can see there is little variation in the response time with grating

wavevector.

These results indicate that, as a result of reduction, the free carrier lifetime has increased and since the response time is inversely proportional to the free carrier lifetime the photorefractive response time has diminished. The free carrier lifetime is inversely proportional to the recombination rate coefficient and the number density of recombination centers, i.e.,

$$\tau = \frac{1}{\gamma_r N_r}. \tag{7}$$

When reduced the concentration of Co^{3+} diminishes and the concentration of Co^{2+} increases. If Co^{3+} are recombination centers in the as-grown crystal then their number density has diminished and the free carrier lifetime will increase as we have determined.

The photorefractive sensitivity, or index change per unit energy absorbed per unit volume, of these crystals can be determined using the formula given in reference [20] as,

$$S = \frac{\gamma\lambda}{4\pi\alpha I\tau}, \tag{8}$$

where γ is the gain coefficient, λ is the wavelength of light, α is the absorption coefficient, I is the incident intensity, and τ is the response time. Shown in Table 2 is the photorefractive sensitivity for various oxides. The first three crystals are 0°-cut samples where the sensitivity has been determined with ordinary polarization and the grating wavevector parallel to the c axis. The first crystal, manganese doped at 100 ppm, is typical of the sensitivity of $BaTiO_3$ prior to this work. The second sensitivity shown is for this same crystal but heated to 120°C, as reported by Rytz et al. [20], which lead to a slight decrease in the gain but large decrease in the response time. The

third sensitivity given is for our reduced crystal. In comparison we conclude that reduction has improved the sensitivity by two orders in magnitude at room temperature. In addition, because the response time is nearly equivalent in the 45°-cut but the gain is much higher the sensitivity is even higher in the 45°-cut and comparable to other photorefractive oxides.

We also reduced a nominally undoped sample that has ~1-2 ppm of iron impurities and found nearly the same absorption feature at ~450 nm. This sample was relatively fast with a beam-coupling rise time of ~10 msec and a peak gain of ~10 cm^{-1} in a 45°-cut. We were able to demonstrate a 30 Hz frame rate (or video frame rate) beam-coupling with this samples as shown in Figure 12. The single trace is initially the signal power with no pump present. When the pump shutter is opened the signal rises to saturation in ~10 msec. The repeated traces are when the pump beam is constantly illuminating the crystal and a signal shutter opens for 25 msec and is closed for 5 msec. When the signal shutter is opened the signal clearly reaches saturation. When the signal shutter is closed the pump beam diffracts off the grating into the signal detector and also erases the grating. (Their is also a small amount of fanned light into the signal direction even after the grating is erased.)

In summary, we have determined the beam-coupling gain and response time in the same n-type $BaTiO_3$ crystal (0° and 45°-cut samples). We obtained equivalent gain in the reduced crystal as compared to the as-grown crystal but found that the response time decreased with a specific reduction state. We have evidence that the response time has decreased in the reduced crystals because the free carrier lifetime has increased. The response time of the 45°-cut was nearly equivalent to the 0°-cut which implies the anisotropy of the mobility is large enough to compensate for the increase in the dc dielectric constant when using a 45°-cut crystal. This implies that the mobility is phonon limited in $BaTiO_3$.

References

1. A. R. Johnson and J. M. Weingart, J. Opt. Soc. Am. **55**(7), 828 (1965).

2. E. Voit, M. Z. Zha, P. Amrhein and P. Günter, Appl. Phys. Lett. **51**(25), 2079 (1987).

3. K. Sayano, A. Yariv, R. R. Neurganokar, Appl. Phys. Lett. **55**(4),328 (1989).

4. F. P. Strohkendl, Ph. D. dissertation, University of Southern California, Los Angeles, CA (1988). (Sample: Cryst. Tech. 1.)

5. J. E. Ford, Y. Fainman, and S. H. Lee, Appl. Opt. **28**(22), 4808 (1989).

6. D. M. Pepper, Appl. Phys. Lett.**49**, 1001 (1986).

7. M. D. Ewbank, R. A. Vazquez, R. S. Cudney, G. D. Bacher, and J. Feinberg, Technical Digest of the OSA Annual Meeting 1990, FS1, Boston, MA.

8. P. Tayebati and D. Mahgerefteh, J. Opt. Soc. Am. B **8**(5), 1053 (1991).

9. J. Feinberg, Photorefractive Materials and Their Applications II, J.-P. Huignard and P. Günter Eds., Springer-Verlag.

10. S. Ducharme, J. Feinberg, R. R. Neurganokar, IEEE JQE QE-23(12), 2116 (1987).

11. Measured by P. Tournois at MIT on a nominally undoped $BaTiO_3$.

12. M. H. Garrett, J. Y. Chang, H. P. Jenssen, Ferroelectrics, (1991).

13. M. Zgonik and P. Günter, Proceedings of the OSA Topical Meeting on Photorefractive Materials Effects, and Devices, TuC13-1, Beverely, MA (1991).

14. J. Hong, P. Yeh, D. Psaltis, and D. Brady, Opt. Lett.**15**(6), 344 (1990).

15. G. C. Valley and M. B. Klein, Opt. Eng. **22**, 704, (1983).

16. D. Mahgerefteh, D. Kirillov, and J. Feinberg, OSA Annual Meeting MJ4, San Jose, CA, Nov. (1991).

17. T. Chang, Ph. D. dissertation, University of Southern California, Los Angeles, CA (1986).

18. C. N. Berglund and W. S. Baer, Phys. Rev. **157**(2), 358 (1967).

19. T. Bogess, G. C. Valley,

20. D. Rytz, M. B. Klein, R. A. Mullen, R. N. Schwartz, G. C. Valley, and B. A.

Wechsler, Appl. Phys. Lett. 52, 1759 (1988)

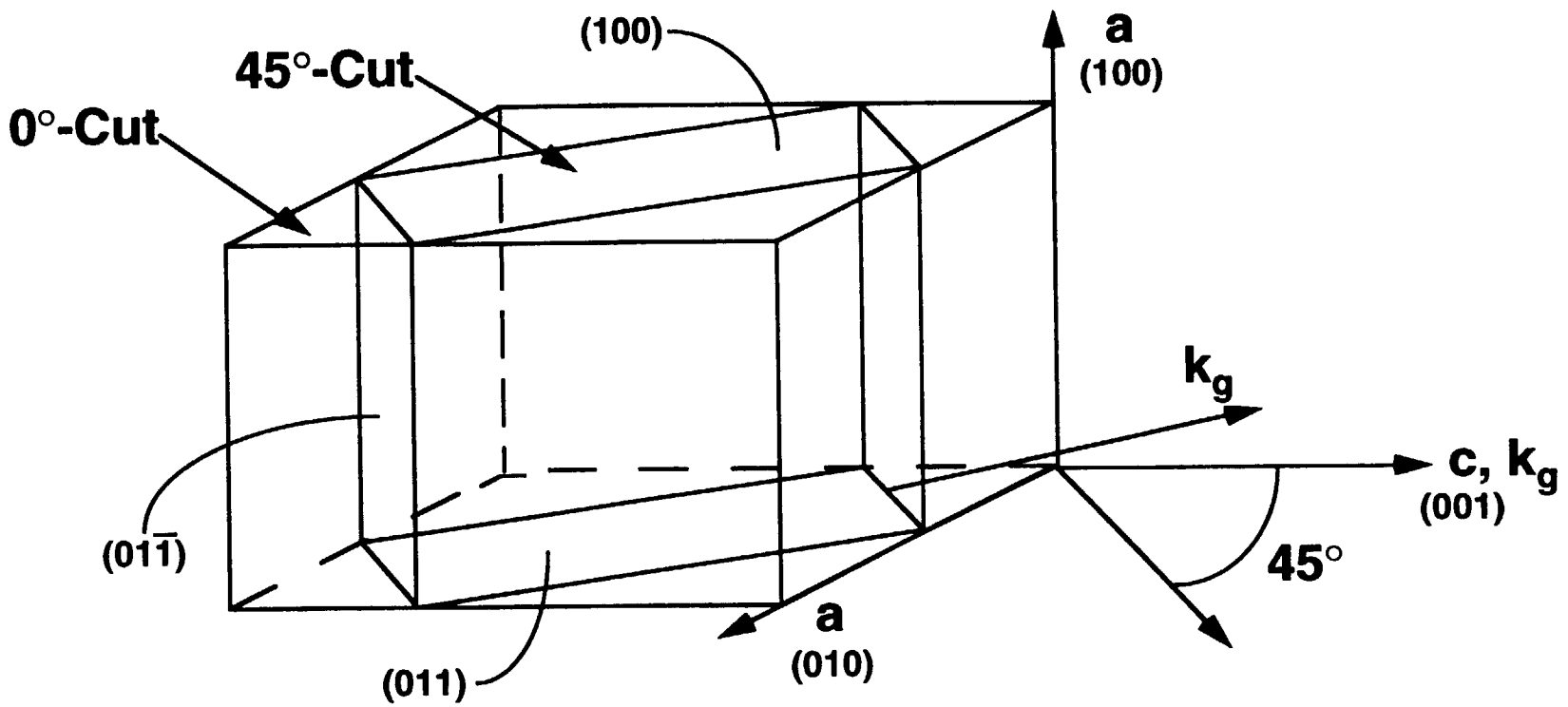

Figure 1. Diagram of the crystallographic orientations and directions of the grating wavevectors k_g for the 0° and 45°-cuts.

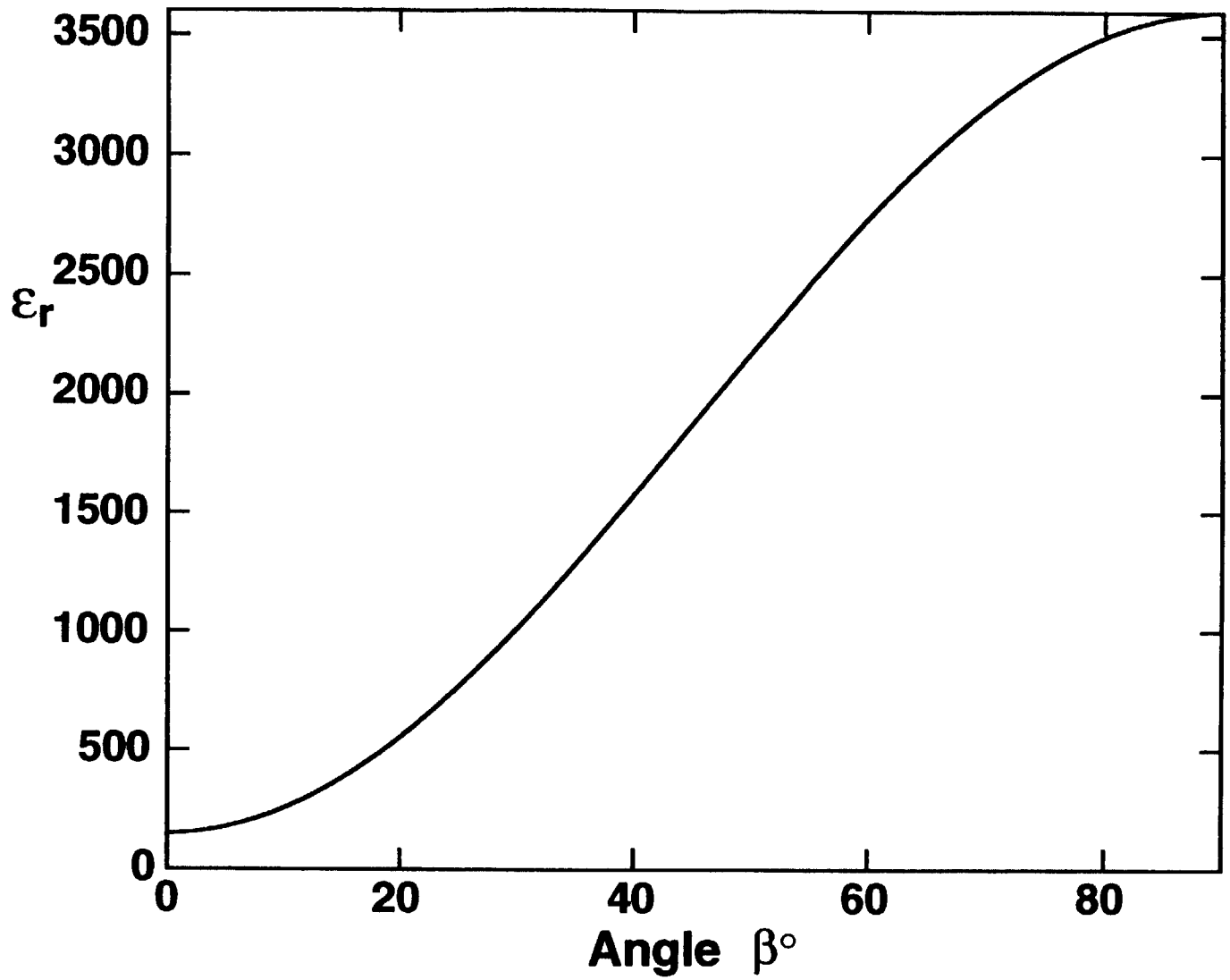

Figure 2. Anisotropy of the dc dielectric constant with respect to the angle between the c-axis and the grating wavevector.

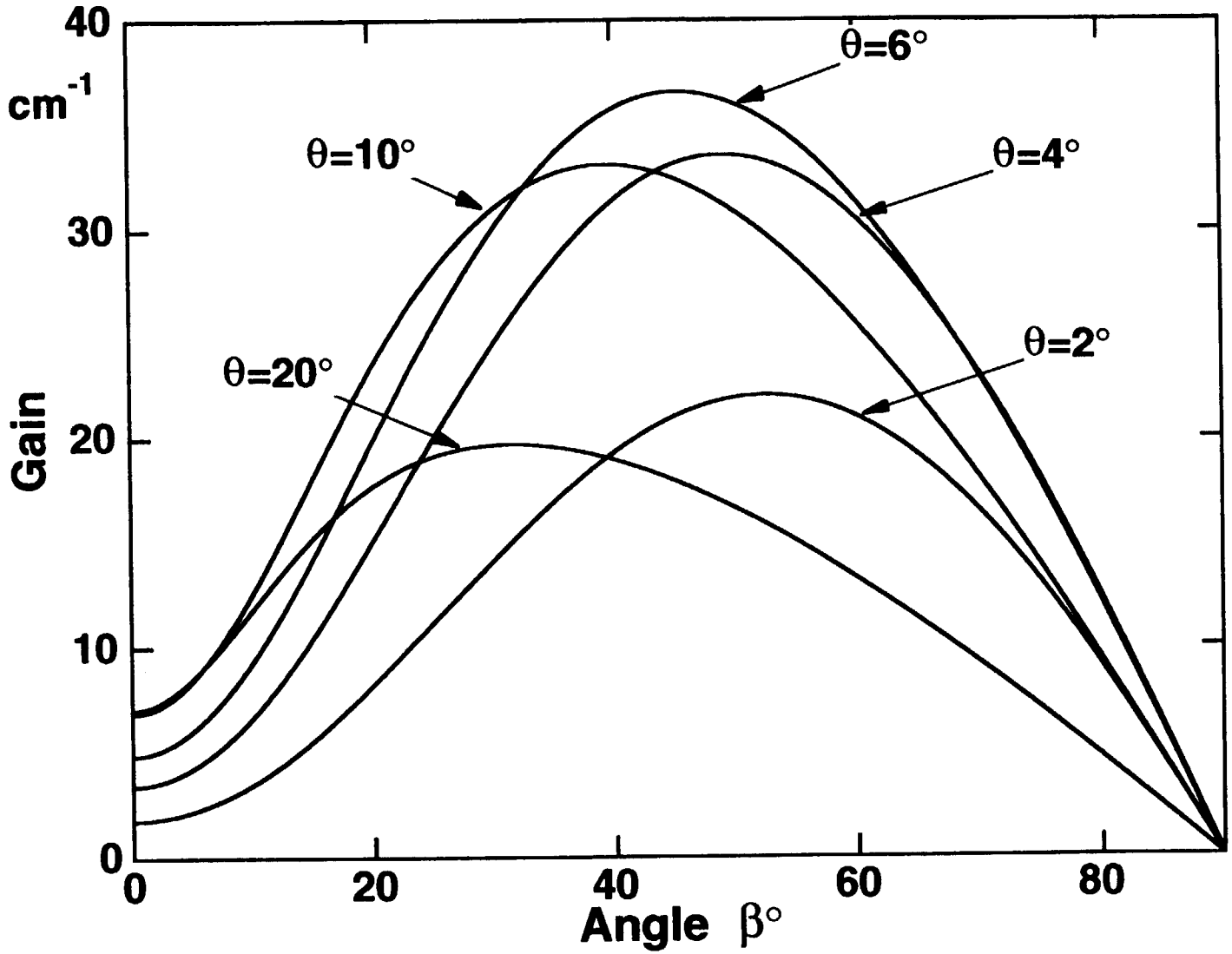

Figure 3. Theoretical beam-coupling gain as a function of the angle between the c-axis and the grating wavevector, β, and with respect to the half-angle between the grating writing beams, θ.

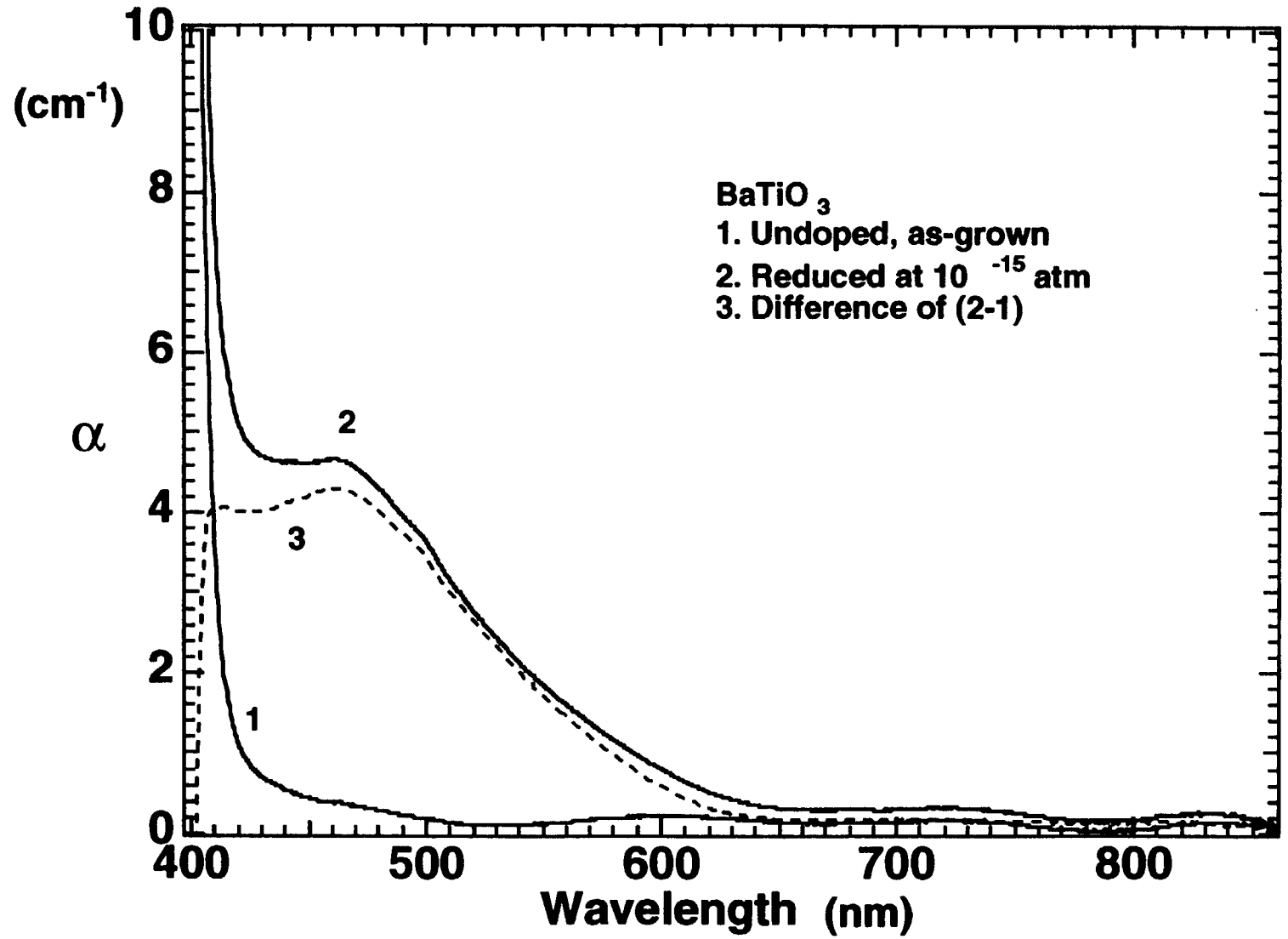

Figure 4. Absorption spectra of oxygen-reduced 20 ppm cobalt-doped barium titanate , barium titanate grown from purified source materials, and their difference spectra.

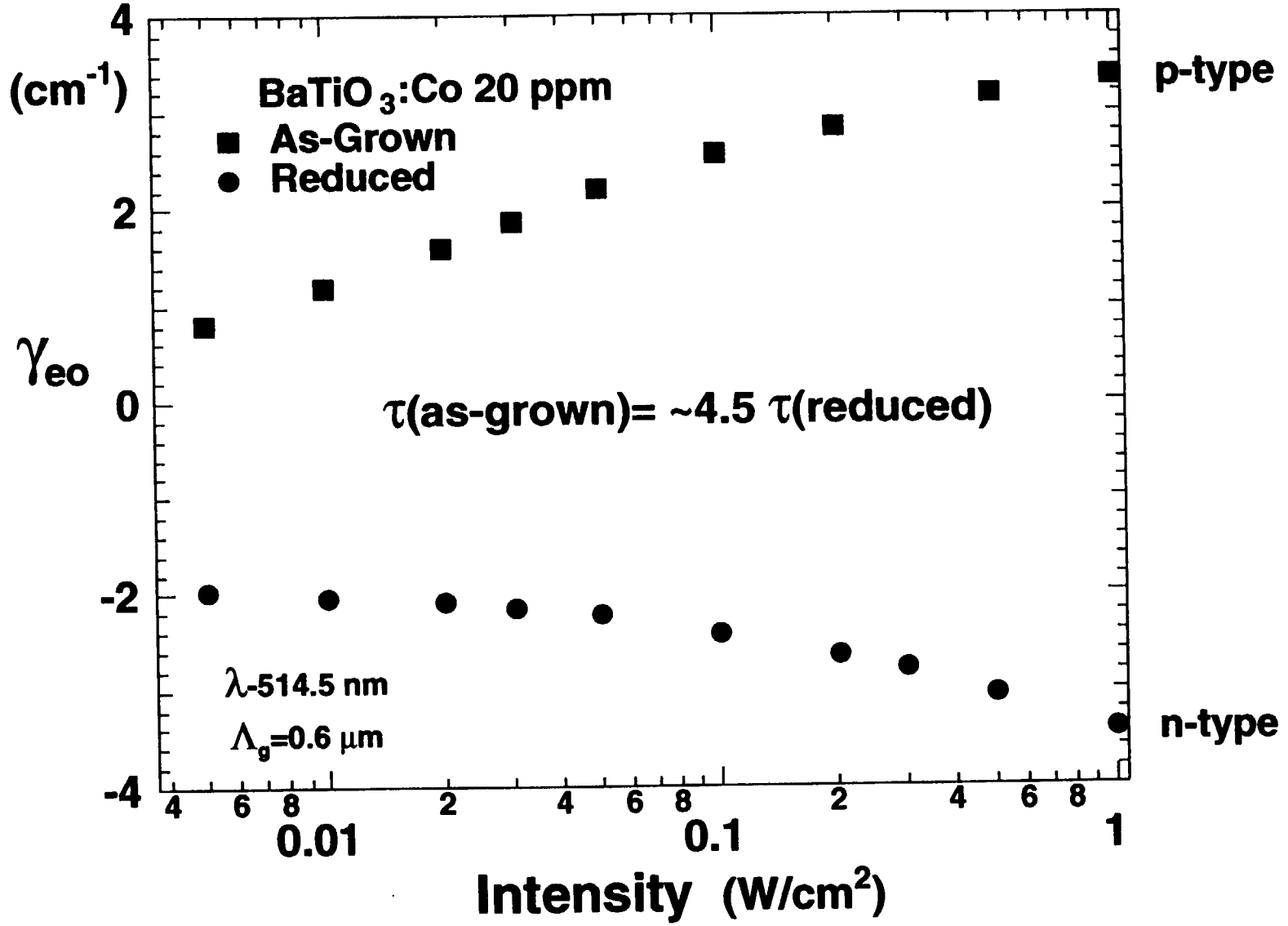

Figure 5. Electrooptic beam-coupling gain as a function of intensity for cobalt-doped barium titanate, as-grown and reduced. The response time of the reduced crystal is approximately 1/4.5 of the response time of the as-grown crystal.

Table 1. Theoretical and experimental values of the beam-coupling gain coefficient as a function of the crystallographic cut, polarization, crystal thickness and grating writing beams ratio. Fanning effects with extraordinary polarized illumination limited the gain measurement accuracy producing a repeatability uncertainty of at least $\pm 2.5\ cm^{-1}$.

	Theory	Experiment	Thickness	Beam Ratio
γ(45°, ord.)	$0.68\ cm^{-1}$	$1.1\ cm^{-1}$	0.87 mm*	800
γ(0°, ord.)	$3.65\ cm^{-1}$	$3.62\ cm^{-1}$	4.52 mm*	800
γ(0°, extra.)	$15.6\ cm^{-1}$	$10.0\ cm^{-1}$	3.40 mm	10^4
γ(45°, extra.)	$32.5\ cm^{-1}$	$26.7\ cm^{-1}$	0.87 mm*	10^4-10^5

*same crystal

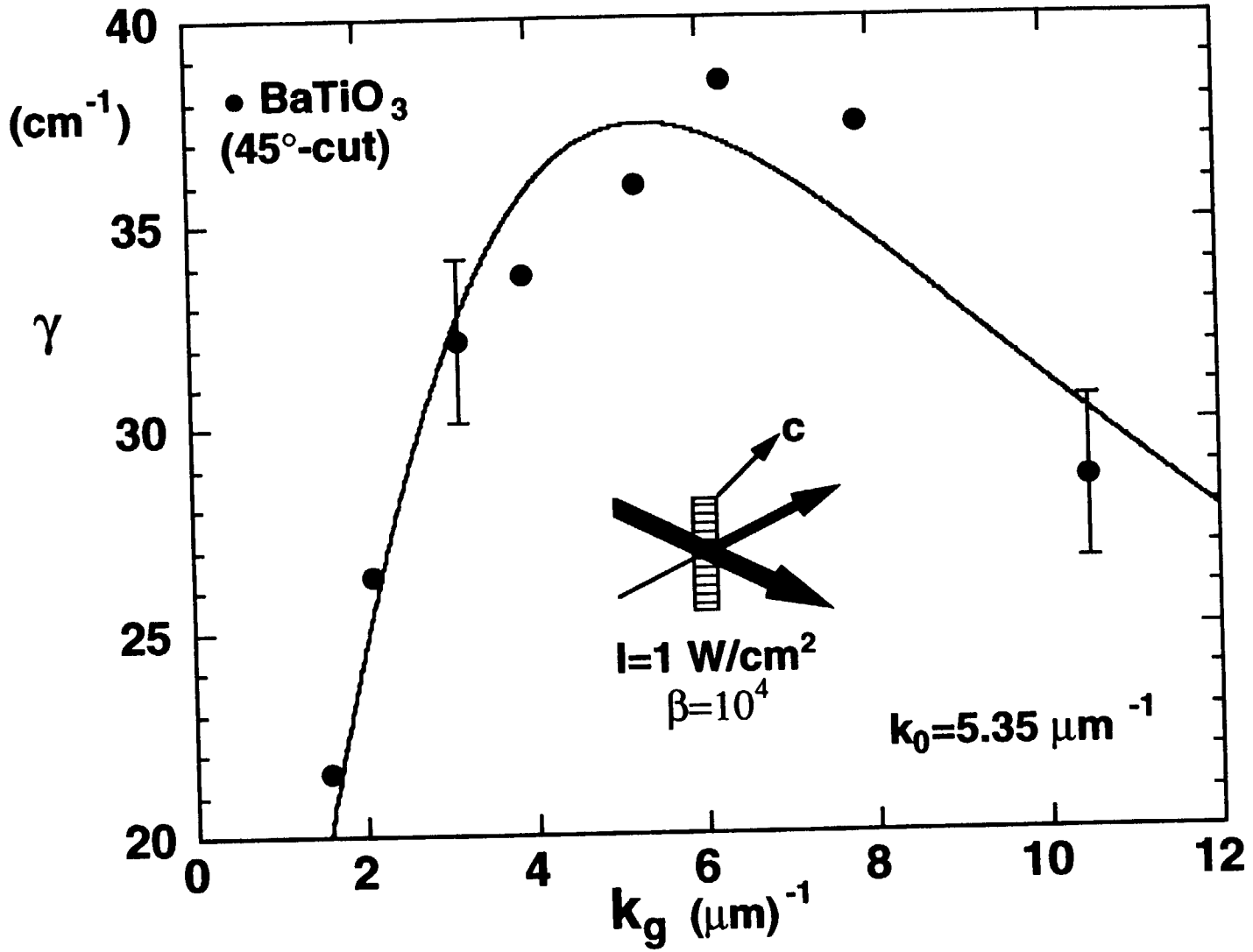

Figure 6. Plot of the beam-coupling gain for a 45°-cut n-type $BaTiO_3$ crystal.

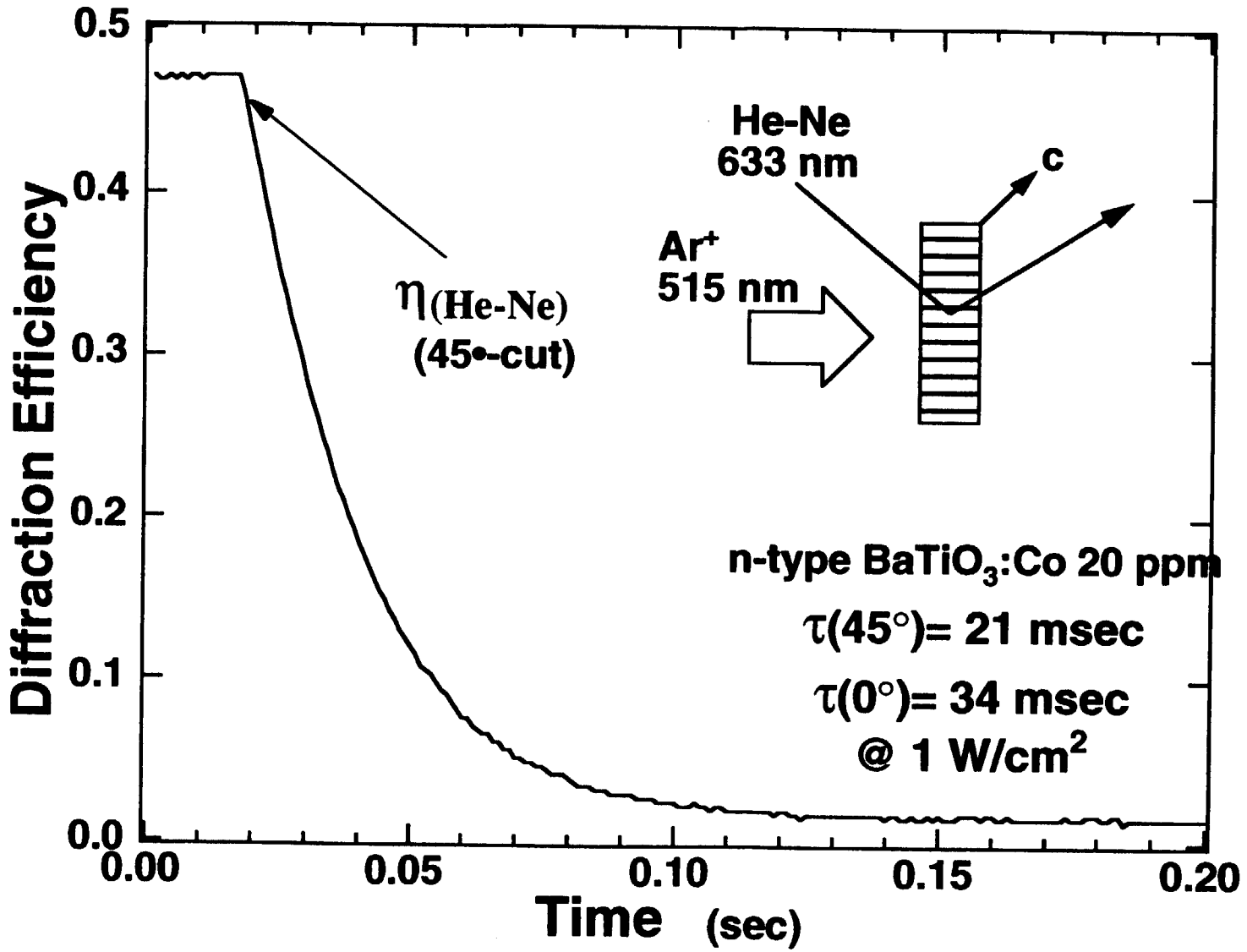

Figure 7. Diffracted light amplitude of a He-Ne readout beam when the grating, written by 514.5 nm illumination of 1 W/cm^2 intensity, is erased by a beam of 1 W/cm^2. This is the decay plot for the 45°-cut crystal.

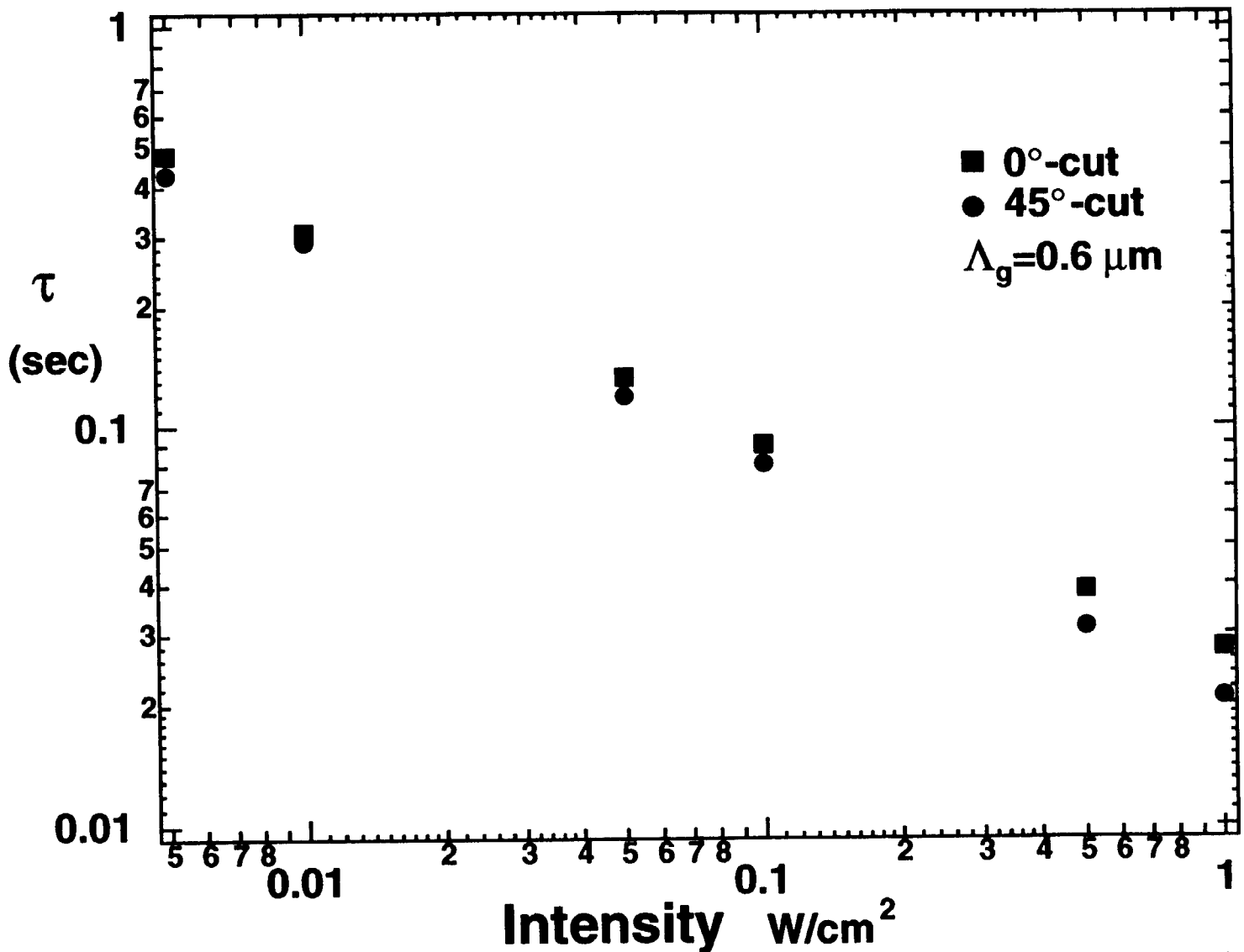

Figure 8. Response time as a function of the writing beam intensity for the same cobalt-doped reduced barium titanate crystal but first in a 0-cut and then in a 45°-cut orientation. The response times are nearly equivalent in both orientations.

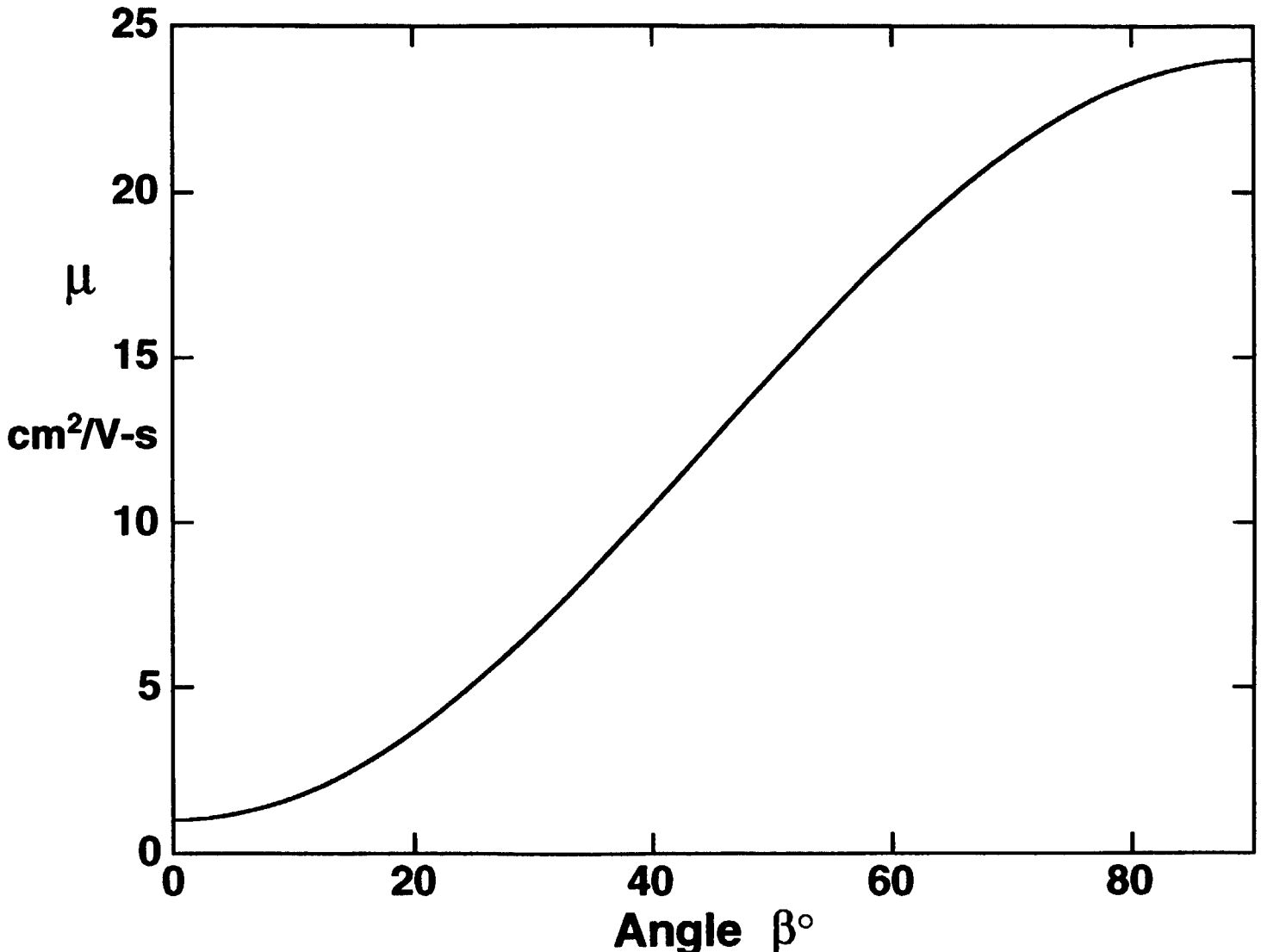

Figure 9. Plot of the anisotropy of the mobility as a function of the angle between the -axis and the grating wave vector assuming the mobility is 1 cm^2/V-sec is the c-direction and that the ratio of the dc dielectric constant to the mobility remains constanat with crystallographic orientation.

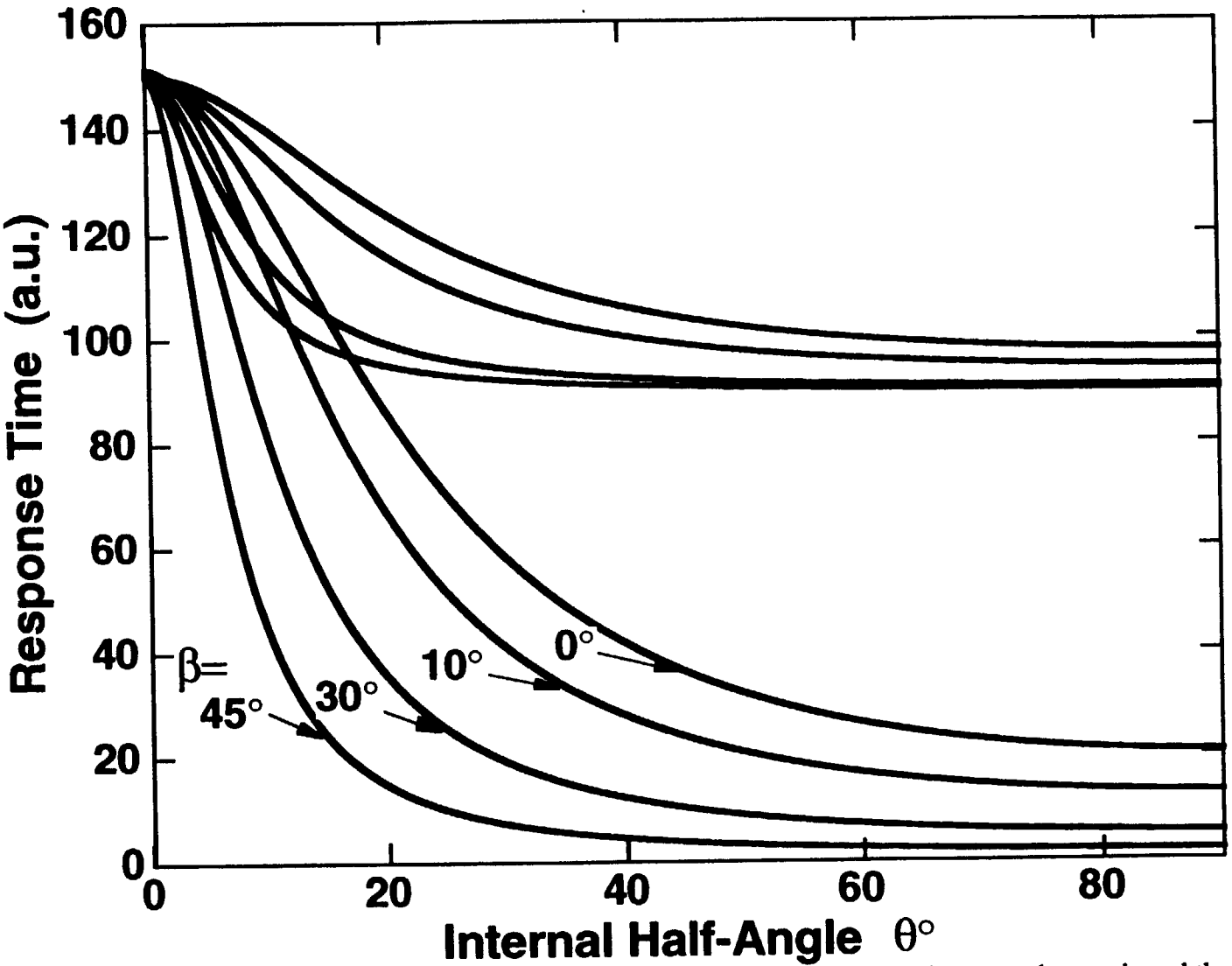

Figure 10. Theorectical plots of the response time as a function of the angle between the c-axis and the grating wavevector and the half-angle between the grating writing beams incorporating changes in the dc dielectric constant and the mobility.. The lower set of curves correspond to a free carrier lifetime of .100 nsec and the upper curves to a free carrier lifetime of 2.5 nsec. Changes in the two sets of curves are from an increase in the mobility-lifetime porduct making the carrier diffusion length comparable to the grating period.

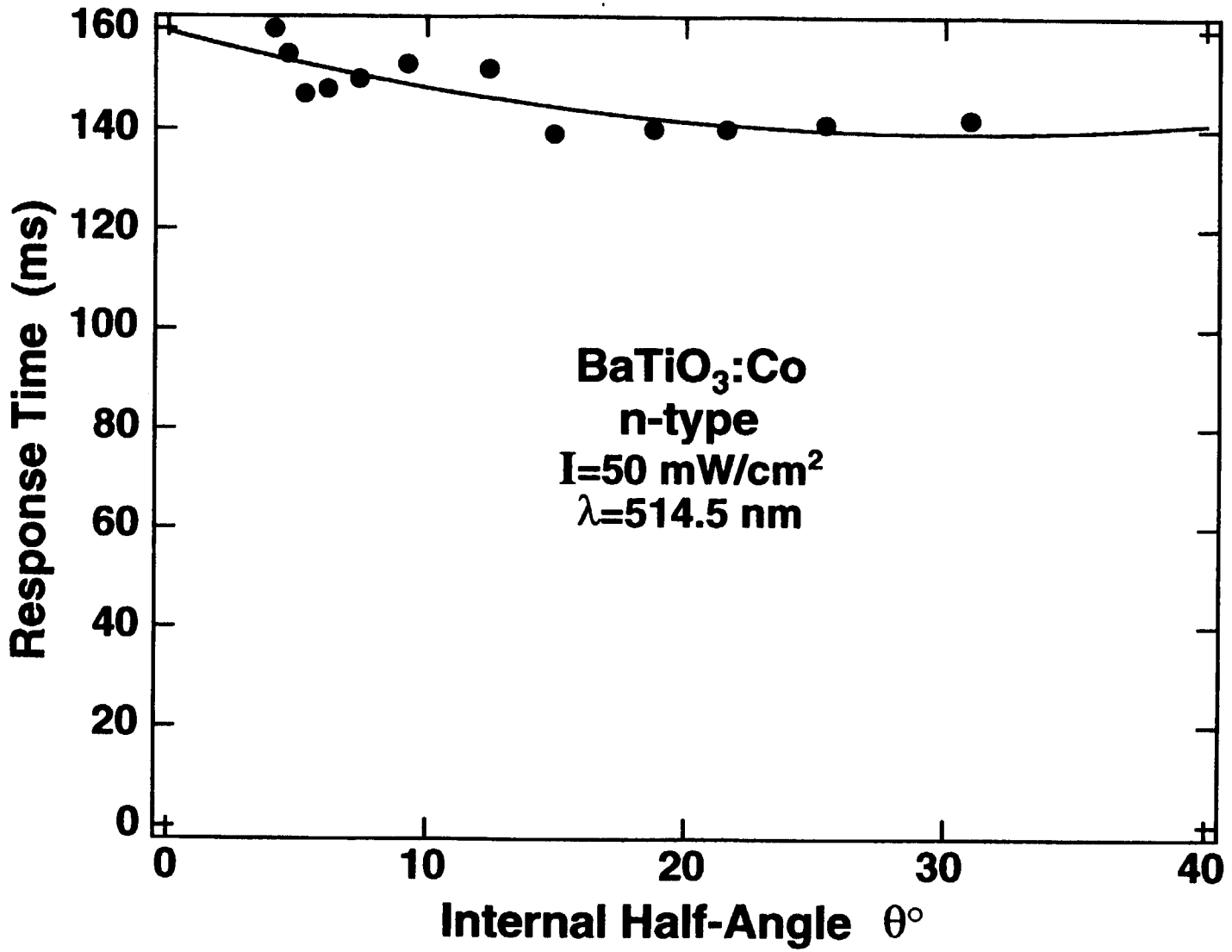

Figure 11. Experimental data points of the response time as a function of half-angle between the gratintg writing beams.

Table 2. Photorefractive properties of various oxide crystals.

Xtal	λ (nm)	α (cm^{-1})	γ (cm^{-1})	τ (msec)	I (W/cm^2)	S (cm^3/kJ)
0° $BaTiO_3$:Mn	514.5	-	~2.5	~1000	2.5	0.002
0° $BaTiO_3$:Mn (120 °C)	514.5	-	~2.2	~15	2.5	0.05
0° $BaTiO_3$:Co (reduced)	514.5	2.2	3.62	34	1.0	0.198
45° $BaTiO_3$:Co (reduced)	514.5¥	2.2	38.7	21	1.0	3.44
SBN:Ce	514.5¥	1.0	~36	333	1.0	0.44
KNb:Fe (reduced)	514.5	1.0	2.5	3.0†	1.0	3.41
BSO	514.5	~0.8	~0.2	0.1	1.0	10.0

¥extraordinary polarization †beam-coupling rise time

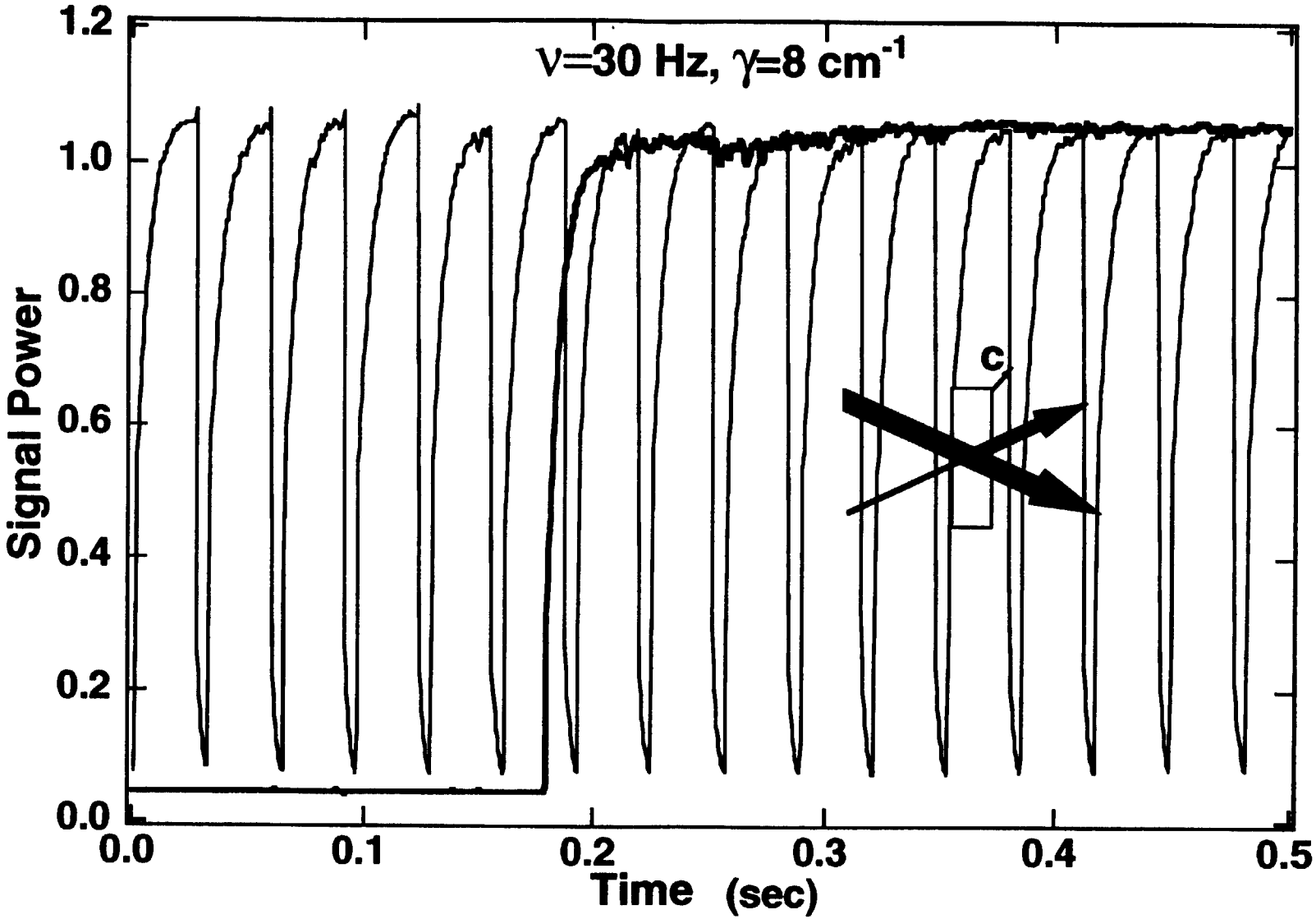

Figure 12. Measurement of the beam-coupling signal power as a function of time. The single trace is the transmitted signal without the pump and then the pump shutter is opened. The signal rises to saturation in approximately 10 msec. The continuous repeating trace is of the signal power when first its shutter is open and beam-coupling occurs. Then, the signal shutter is closed and the pump beam erases the grating. This is repeated at a 30 Hz rate and the beam-coupling gain is approximately >8 cm^{-1}.

8 Summary and Conclusions

In summary, we have investigated the crystal growth and photorefractive properties of reduced n-type $BaTiO_3$:Co, and the effect of crystallographic orientation on the response time and beam-coupling gain. In the process we have optimized the growth of barium titanate producing cap free boules, invented a new method to pole barium titanate especially important for high conductivity crystals, and developed a new method to measure the absorptive and electrooptic gain. We have found a reduction level that we believe increased the free carrier lifetime and thus reduced the response time of barium titanate. We found that the mobility scaled with the dc dielectric constant and thus infer that the mobility is phonon limited in barium titanate. We have produced barium titanate crystals that have the fastest response time at room temperature (~21 msec at 1 W/cm^2), high gain (38.7 cm^{-1}), and the highest photorefractive sensitivity (3.44 cm^3/kJ) reported to date. In addition, we have demonstrated beam-coupling at video frame rates.

In conclusion, we have made significant progress and developed of high performance photorefractive barium titanate crystals. Real-time photorefractive applications will become viable with the materials developed by this research. Since the speed of response varies with reduction level and impurity concentration we suspect that dopants play a role in the type of defect center, i.e., their recombination rate coefficient and trap density, and therefore will also modify the free carrier lifetime. Therefore, further improvement in the performance of $BaTiO_3$ is possible by optimizing the reduction as a function of the dopant type and concentration.

9 List of Publications and Conferences

9.1 Publications

1. M. H. Garrett, J. Y. Chang, H. P. Jenssen and C. Warde, "High Photorefractive Sensitivity in a n-type $BaTiO_3$ Crystal," Opt. Lett., Jan. 1991.

2. J. Y. Chang, M. H. Garrett, H. P. Jenssen and C. Warde, "Sublinear Intensity Dependence of the Response Time, Light-Induced Dark Decays, and the Photorefractive Sensitivity of Cobalt-Doped Barium Titanate, $BaTiO_3$:Co," Submitted to JOSA B.

3. M. H. Garrett, J. Y. Chang, H. P. Jenssen and C. Warde, "High Beam-Coupling Gain in Cobalt-Doped Barium Titanate, $BaTiO_3$:Co," Submitted to JOSA B.

4. M. H. Garrett, J. Y. Chang, H. P. Jenssen and C. Warde, "A method to pole barium titanate, $BaTiO_3$," Ferroelectrics **120**, 167 (1991).

5. M. H. Garrett, J. Y. Chang, P. Tayebati, H. P. Jenssen, C. Warde, "The Influence of Cobalt-Doping on Deep and Shallow Trap Dependent Photorefractive Properties of Barium Titanate," Proceedings of the OSA Topical Meeting on Photorefractive Materials, Effects & Devices, Beverely, MA, 1991.

6. M. H. Garrett, J. Y. Chang, H. P. Jenssen , C. Warde, and T. Pollak, "Photorefractive and Photochromic Effects in Barium Titanate," Proceedings of the OSA Topical Meeting on Photorefractive Materials, Effects & Devices, Beverely, MA, July 29-31, 1991.

7. M. H. Garrett, J. Y. Chang, H. P. Jenssen and C. Warde, "Optimizing the Photorefractive Properties of Barium Titanate, $BaTiO_3$," Proceedings of the OSA Topical Meeting on Photorefractive Materials, Effects, and Devices Topical Meeting PD8, OSA, Beverely, MA, July 29-31, 1991.

8. M. H. Garrett, J. Y. Chang, H. P. Jenssen and C. Warde, "Photochromic-Induced Photorefractive Changes in Barium Titanate," Proceedings of the MRS Meeting, Anaheim, CA April, 1991.

9. J. Y. Chang, M. H. Garrett, P. Tayebati, H. P. Jenssen, C. Warde, "Photorefractive Properties of Cobalt-Doped Barium Titanate," Proceedings of the MRS Meeting, Anaheim, CA April, 1991.

10. Thomas P. Dougherty, Gary P. Wiederrecht, Mark H. Garrett, H. P. Jenssen, C. Warde and Keith A. Nelson, "Femtosecond Impulsive Stimulated Raman Scattering Study of Soft-Mode and Order-Disorder Dynamics in Tetragonal $BaTiO_3$" Submitted to Phys. Rev. B.

11. Thomas P. Dougherty, Gary P. Wiederrecht, Mark H. Garrett, H. P. Jenssen, C. Warde and Keith A. Nelson, "Femtosecond Time-resolved Observation of Soft Mode Dynamics in Structural Phase Transitions," Submitted to Phys. Rev. Lett.

9.2 Conferences

1. M. H. Garrett, J. Y. Chang, H. P. Jenssen and C. Warde, "Fast Response Times and High Photorefractive Sensitivity in an n-type $BaTiO_3$ Crystal," OSA Annual Meeting, San Jose, California, PD-23, Nov. 1991.

2. M. H. Garrett, J. Y. Chang, H. P. Jenssen, C. Warde, and T. M. Pollak, "Photorefractive and Photochromic Effects in Barium Titanate, $BaTiO_3$," Photorefractive Materials, Effects, and Devices Topical Meeting, OSA, Beverely, Massachusetts, July 29-31, 1991.

3. M. H. Garrett, J. Y. Chang, H. P. Jenssen and C. Warde, "The Influence of Cobalt-Doping on Deep-and-Shallow Trap Dependent Photorefractive Properties of Barium Titanate," Photorefractive Materials, Effects, and Devices Topical Meeting, OSA, Beverely, Massachusetts, July 29-31, 1991.

4. M. H. Garrett, J. Y. Chang, H. P. Jenssen and C. Warde, "Optimizing the Photorefractive Properties of Barium Titanate, $BaTiO_3$," Photorefractive Materials, Effects, and Devices Topical Meeting PD8, OSA, Beverely, Massachusetts, July 29-31, 1991.

5. M. H. Garrett, J. Y. Chang, and C. Warde, "Photochromic Enhancement of the Photorefractive Effect in Barium Titanate," MRS Meeting, Anaheim, CA, April 29, 1991.

6. J. Y. Chang, M. H. Garrett, and C. Warde, "Photorefractive Properties of Cobalt-Doped Barium Titanate," Materials Research Society Meeting, Anaheim, CA, April 29, 1991.

7. M. H. Garrett, J. Y. Chang, H. P. Jenssen, H. L. Tuller and C. Warde, "Photorefractive two-beam-coupling in barium strontium titanate, $Ba_{1-x}Sr_xTiO_3$," Optical Society Annual Meeting, Boston, Massachusetts, Nov. 1990.

8. P. Tayebati, M. H. Garrett and J. Y. Chang, "Hole-electron competition and shallow traps in the photorefractive effect," Optical Society Annual Meeting, Boston, Massachusetts, Nov. 1990.

9. M. H. Garrett, J. Y. Chang, H. P. Jenssen, H. L. Tuller and C. Warde, "Top-Seeded Solution Growth and Photorefractive Characterization of Barium Strontium Titanate, $Ba_{1-x}Sr_xTiO_3$," Proceedings of the American Conference of Crystal Growth - 8, Vail, Colorado, July 1990.